Estimation of road frictional force and wheel slip for effective Anti-lock Braking System (ABS) control

Sulakshan Rajendran[1] Sarah K Spurgeon[1,*] Georgios Tsampardoukas[2]
Ric Hampson[2]

[1]Department of Electronic and Electrical Engineering, University College London, UK
[2]Jaguar Land Rover, W/1/26 Abbey Road, Whitley, Coventry, CV3 4LF, UK

SUMMARY

The introduction of electric braking via brake-by-wire systems in Electric Vehicles (EVs) has reduced the high transportation delays usually involved in conventional friction braking systems. This has facilitated the design of more efficient and advanced control schemes for Anti-lock Braking Systems (ABS). However, accurate estimation of the tyre-road friction coefficient, which cannot be measured directly, is required. This paper presents a review of existing estimation methods focusing on sliding mode techniques, followed by the development of a novel friction estimation technique which is used to design an efficient ABS control system. This is a novel slip-based estimation method which accommodates the coupling between the vehicle dynamics, wheel dynamics and suspension dynamics in a cascaded structure. A Higher Order Sliding Mode Observer (HSMO) based scheme is designed considering the nonlinear relationship between friction and slip. A first order Sliding Mode Observer (SMO) is also designed based on a purely linear relationship. A key feature of the proposed estimation schemes is the inclusion of road slope and the effective radius of the tyre as an estimated state. These parameters impact significantly on the accuracy of slip and friction estimation. The performance of the proposed estimation schemes are validated and benchmarked against a Kalman Filter (KF) by a series of simulation tests. It is demonstrated that the sliding mode observer paradigm is an important tool in developing next generation ABS systems for EVs.

KEY WORDS: ABS control, adaptive estimation, sliding mode observers

Nomenclature

$\omega\ \omega_v$	*Wheel angular speed and wheel speed*
μ	*Friction coefficient*
$\mu_x\ \mu_y$	*Longitudinal and lateral friction coefficient*
$\mu_{max}\ \mu_s$	*Peak friction coefficient and sliding friction coefficient*
$\lambda\ \lambda^d$	*Actual and desired wheel slip*
$\lambda_f\ \lambda_r$	*Front and rear wheel slip*
I	*Moment of inertia*
v	*Vehicle velocity*
$v_x\ v_y$	*Longitudinal and lateral components of velocity*
$F_x\ F_y\ F_z$	*Longitudinal, lateral and vertical forces*

---

*Correspondence to: Sarah K Spurgeon *Department of Electronic and Electrical Engineering, University College London, UK*
†E-mail: s.spurgeon@ucl.ac.uk

s_x *Longitudinal sheer stress*

L_c *Length of contact patch*

T_b *Brake torque*

R *Tyre radius*

$R_o\ R_e\ R_s$ *Free rolling, Effective and static tyre radius*

$D_p\ B\ C\ E$ *Magic Formula coefficients*

$z_s\ z_u$ *Vertical displacements of sprung and unsprung masses*

m *Vehicle mass*

$m_s\ m_u$ *Sprung and unsprung masses*

$\theta\ \phi\ \psi$ *Pitch, roll and yaw of vehicle*

θ_s *Road slope*

β *Side slip*

$L_f\ L_r$ *Distances from CoG to front and rear wheels*

L_w *Wheel base*

$K_s\ B_s$ *Spring and Damp constants of sprung mass*

K_r *Constant of unsprung mass*

α_s *Side slip angle*

C_s *Longitudinal tyre stiffness*

C_e *Wheel rolling circumference*

C_r *Coefficient of rolling resistance*

$C_d\ D_a$ *Coefficient of air drag, and lumped term of air drag*

$F_d\ F_r$ *Air drag and rolling resistance forces*

D *Lumped disturbance and uncertainty of HSMO*

d *Disturbance to the system*

Δ *Uncertainty*

IC_R *Instantaneous tyre center*

$a_x\ a_y\ a_z$ *Longitudinal, lateral and vertical acceleration*

L *Switching function*

h *Height of CoG from wheel-road contact center*

$h_f\ h_r$ *Heights of CoG from front and rear wheel-road contact centre*

G_e *Design parameter of tyre force estimator of SMO scheme*

Ω *Slip-friction force ratio factor*

ρ_d *Air density*

ρ_m *Vertical force dependant coefficient of MF*

$\rho\ \Gamma\ \varepsilon$ *Positive design parameters of HSMO*

q *Rate of change in road slope*

l *Adaptive law of HSMO*

σ *Sliding surface*

α *Assist input control of HSMO*

z *State of observer*

δ *Steering angle*

∂ *Change in a state or parameter*

$K\ K_k\ K_{rls}$ *Gains of SMO, KF and RLS algorithm*

1. INTRODUCTION

ABS is an important safety feature in road vehicles during emergency or heavy braking conditions, where it prevents wheel lockup and reduces the braking distance by maximizing the frictional force. The wheel of a road vehicle is likely to slip during severe braking or

braking on a slippery surface such as on an icy road. This increases stopping distances, and sometimes the vehicle may lose steerability. The objective of the ABS system is to control the wheel slip at an optimal value ensuring maximum friction which will achieve shorter stopping distances [1]. Furthermore, ABS indirectly ensures the steerability of the vehicle by preventing wheel lock.

Many state-of-the-art wheel slip controllers described in the literature [2] [3] [4] [5] are limited by the fact that in practical implementation, reliable information on tyre-road friction may not be available. Many controllers disregard this important influence on controller performance in the presence of different road conditions. A robust controller can be developed to overcome the uncertainties in the unmodelled characteristics of the tyre-road interaction but to produce better braking performance, the optimal slip value with respect to the current road conditions should be deployed. Furthermore, many contributions assume the wheel slip is calculated accurately but, in reality, accurate measurement of vehicle velocity is required to achieve this, and this is problematic.

There are a number of ways to overcome this problem. GPS technology can be deployed [6] [7] [8] [9]. However, GPS measurements are not always accurate and even with extremely accurate slip measurement there remains a lack of information available on the friction force that can be transmitted from tyre to road. To obtain this information requires costly force sensors to measure the longitudinal and lateral tyre forces [8]. Information on lateral tyre forces is required to retain control of the vehicle heading (yaw control) when braking in a curve or cornering to avoid an obstacle. Hence, the development of effective estimators to estimate tyre forces which can be used to enhance the performance of ABS control strategies is a topic of continuing research interest.

The ABS control problem can be outlined by appealing to the so-called quarter car model. This model consists of a single wheel attached to a mass, as shown in Figure 1.
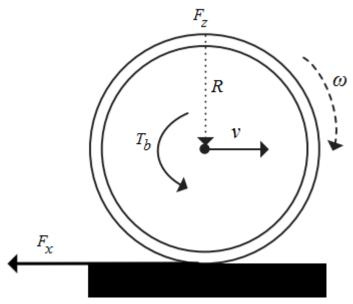

Figure 1. Quarter car model

Figure 1 illustrates the free body diagram of a quarter car vehicle model or a single wheel model of a vehicle undergoing longitudinal braking motion. This model captures the fundamental dynamic characteristics of the system in a simple form that is widely used by

control engineers and researchers [5]. The equations of motion of the quarter car, in the case of braking, are given by:

$$I_\omega \dot{\omega} = RF_x - T_b \tag{1}$$

$$m\dot{v} = -F_x \tag{2}$$

$$F_x = F_z \mu(\lambda) \tag{3}$$

I_ω is the inertia of the wheel, ω is the angular velocity of the wheel, F_x and F_z are the friction and normal force acting on the wheel respectively, v is the vehicle velocity, T_b is the braking torque, μ is the tyre-road friction coefficient and λ is the relative wheel slip which is given as follows

$$\lambda = \frac{v - \omega R}{v} \tag{4}$$

A locked wheel ($\omega = 0$) is described by $\lambda = 1$, while the free motion of the wheel $\omega R = v$ is described by $\lambda = 0$.

Many of the important signals required for the ABS control unit are not directly measurable. Typical variables that require estimation are the tyre slip λ, velocity of the car v and the maximum friction coefficient μ. In fact, slip estimation is based on estimation of the velocity of the car and the angular wheel velocity measured by wheel speed sensors. A typical ABS control structure is shown Figure 2.
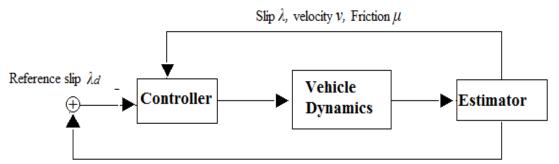

Figure 2. ABS control

The paper first describes the tyre-road interaction dynamics and a review of slip-based friction estimation methods is then presented. This review is structured into two sections; the first presents a general overview of slip-based estimation methods and the second presents a critical discussion of estimation methods focusing on SM based schemes. Two estimation schemes based on HSMO and SMO respectively are then presented to estimate both slip and frictional force. The important feature of the proposed schemes is that wheel, suspension and vehicle dynamics and the couplings between them are all considered. The SMO and HSMO consider a linear and nonlinear relationship between slip and friction respectively, as part of the observer design. A novel HSMO based scheme estimates vehicle velocity by accurately estimating the disturbances. Furthermore, vertical tyre force is estimated using an EKF based on a vertical dynamic integrated model including suspension dynamics considering road slope and vehicle pitch due to severe braking. The effective tyre radius is updated as a function of vertical force and is used to improve slip estimation. The efficacy of the proposed approach is demonstrated using simulation experiments.

2. TYRE-ROAD INTERACTION

Development of an effective friction estimation method demands in-depth understanding of the tyre-road interaction.
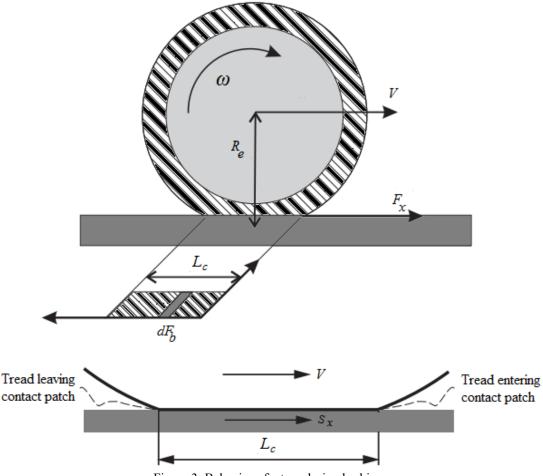

Figure 3. Behavior of a tyre during braking

During braking, the applied braking torque stretches the leading half of the tyre tread due to its elasticity before it enters the contact patch as shown in Figure 3 above, where L_c is the contact patch length and s_x is the longitudinal sheer stress. The qualitative trend of friction coefficient against slip and slip zone illustrations for different values of slip are given in Figure 4. Two important values of the friction coefficient can be identified during driving and braking on the μ-λ curve shown in Figure 4a. They are the peak friction coefficient μ_{max} and the pure sliding coefficient μ_s, respectively. The dashed line is the zone where pure sliding occurs, and the vehicle becomes unstable. The stable-unstable zones of the μ-λ curve will be discussed later in this section. It can be seen from Figure 4b that the slip zone increases to a certain value with increasing slip values and that beyond that value global sliding of the wheel occurs.

The longitudinal tyre travel is high when it is subjected to a braking torque compared to free rolling. This generates a tractive force proportional to the brake torque. The section of the graph marked OA in Figure 5 shows that this tractive force increases linearly until the

elasticity of the tyre is surpassed. The section AB of the curve describes the sliding
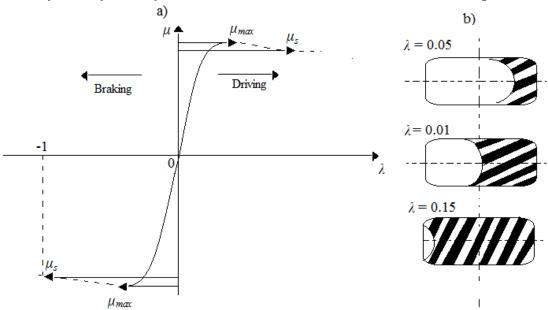

Figure 4. a) Qualitative trend of friction coefficient as a function of slip b) slip zone of the tyre-road contact with different slip values. (adopted from [10]).

of the tyre and during sliding the tractive force varies nonlinearly with longitudinal slip. If the braking torque is increased further, the tractive force plunges from a peak to a much lower value when the wheel locks (i.e. at slip 1.0) as described by the segment BC.
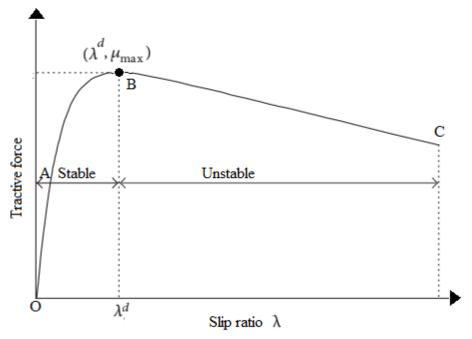
Figure 5. Tractive force wheel slip (λ)

Jiang [11] and Savaresi [12] stated that open loop braking is stable for the increasing part of the curve in Figure 5 and unstable for the decreasing part of the curve. When the brake torque T_b, is applied, the wheel speed decreases while the wheel slip increases. Then the tractive force produced by the road increases the wheel speed which decreases the wheel slip. In the

increasing part of the $\mu - \lambda$ curve, an increase in wheel slip produces a high tyre force due to high μ which then causes a drop in wheel slip.

However, in the decreasing part of the $\mu - \lambda$ curve, an increase in wheel slip produces a lower tyre force due to a low value of μ which leads to a continuous rise in the wheel slip. Therefore, the peak point of the $\mu - \lambda$ curve is critical.
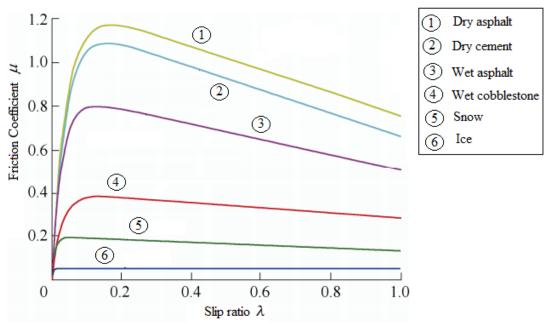

Figure 6. $\mu - \lambda$ curves for different road surfaces

The position of the peak value of the $\mu - \lambda$ curve or the maximum friction coefficient varies for different road conditions as shown in Figure 6. Thus, the optimal wheel slip is also different for different conditions.
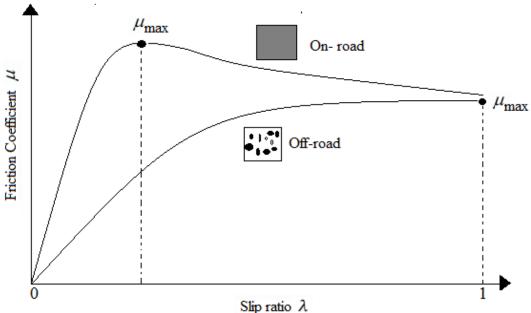

Figure 7. $\mu - \lambda$ curves for on and off-road conditions

The optimal wheel slip ratio for the majority of road surfaces is approximately between 0.1 to 0.3 [9] and many of the control strategies published in the literature focus on maintaining a wheel slip of around 0.2 to achieve optimal braking [1] [2].

The maximum friction potential occurs at slip $\lambda = 1$ when braking during off-road conditions such as on soft soil. This is because of the increasing rolling resistance and the so-called *bulldozing effect*. Under soft terrain conditions, the tyre sinks due to tyre load and shear displacement. At high-slip, tyre sinkage develops additional lateral force at the tyre wall and this is called the bulldozing effect. This effect increases cornering stiffness and the friction potential [13] [14] [15]. The $\mu - \lambda$ curves for road and off-road conditions are illustrated in Figure 7.

2.1 Tyre-model / Magic Formula (MF)

Tyre-road interaction is very complex and important in vehicle dynamics and load analysis. Extensive research has been carried out on vehicle dynamics and tyre models in past decades. Tyre models are usually classified into three types based on their applications. They are tyre models for handling analysis, ride comfort analysis and durability analysis, respectively. A detailed comparison between tyre models is presented in [16]. The most widely used tyre model in industry is the Magic Formula (MF), and hence it is used in this study. This is a semi-empirical model developed by Pacejka [17] based on real experimental data and the parameters are not the physical properties of the tyre. The general form of the model is given by

$$Y = D_p \sin\left[C \tan^{-1}\left(Bx - E(Bx - \tan^{-1}(Bx))\right)\right] \qquad (5)$$

where Y denotes the tyre force, B is the stiffness factor, C is the shape factor, D_p is the peak value and E is the curvature factor.

Equation (5) can be used for both longitudinal and lateral force calculations. The MF can be re-written for combined slip conditions as follows:

$$F_x = G_{xa}F_{\lambda x} \text{ and } F_y = G_{yk}F_{\lambda y} \qquad (6)$$

where

$$G_{xa} = \cos\left(C_{xa}\tan^{-1}(B_{xa}\tan\alpha)\right) \text{ and } G_{ya} = \cos\left(C_{ya}\tan^{-1}(B_{ya}k)\right)$$

$F_{\lambda y}$ and $F_{\lambda x}$ represent the longitudinal and lateral tyre forces respectively in pure slip conditions and $C_{xa,}$ $B_{xa,}$ $C_{ya,}$ and B_{ya} are additional coefficients corresponding to the combined slip condition. Hence, the model equations for combined slip conditions are given as

$$F_x = \cos\left(C_{xa}\tan^{-1}(B_{xa}\tan\alpha)D_{px}\sin\left(B_x k - E_x(B_x k - \tan^{-1}(B_{xk}))\right)\right) \qquad (7)$$

$$F_y = \cos\left(C_{ya}\tan^{-1}(B_{yak})D_{py}\sin\left(C_y^{-1}tan\left(B_y\tan\alpha - E_y\left(B_y\tan\alpha - \right.\right.\right.\right.$$
$$\left.\left.\left.\left.\tan^{-1}(B_y\tan\alpha)\right)\right)\right)\right) \qquad (8)$$

Equations (7) and (8) can be used to estimate F_x, μ_x and F_y, μ_y, respectively. Distinct μ_x and μ_y depend on the longitudinal and lateral properties of the tyre-road interaction [59]. The

actual relationship between μ_x and μ_y is illustrated by the ellipse given in Figure 8a. However, [18] and [19] suggest that the friction ellipse can be assumed to be a circle as illustrated in Figure 8b. In this case, it can be assumed that $\mu = \mu_x = \mu_y$. The assumption that the friction ellipse is a circle is not valid when the excitation of the lateral dynamics is significant. Weighted average values of μ_x and μ_y estimated independently can be used to obtain more accurate estimates of μ for different driving scenarios, which will be particularly important when the balance of the impact of the lateral and longitudinal dynamics is varying:

$$\hat{\mu} = \sum \hat{\mu}_x \frac{|F_x|}{|F_x| + |F_y|} + \hat{\mu}_y \frac{|F_y|}{|F_x| + |F_y|} \qquad (9)$$
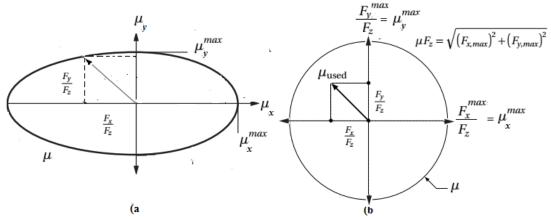

Figure 8. a) Actual friction ellipse b) Assumed friction circle

3. FRICTION ESTIMATION METHODS

In recent decades, there has been an intensive effort from the international research community to develop efficient methods to estimate the tyre-road friction coefficient and slip. In Europe, projects such as "*Prometheus*" and "*Friction*" have been conducted . "*Prometheus*" focused on fully autonomous driving by installing sensors to enable the vehicle to adapt to the road conditions [21] [22]. "*Friction*" investigated effective sensor-fusion for friction coefficient estimation [45]. In general, friction estimation methods are classified based on the sensor requirements and the level of excitation of the vehicle dynamics. The classification of methods is illustrated in Figure 9.

So called cause-based approaches are based on the factors that influence the friction coefficient whereas the effect-based approaches focus on the variables that are affected by the friction coefficient. Uchanski [23], Lex [24] and Chang [25] present detailed reviews on friction estimation methods. In this work, friction estimation schemes are developed based on wheel slip, hence, the literature concerning slip-based estimation methods is the focus here.
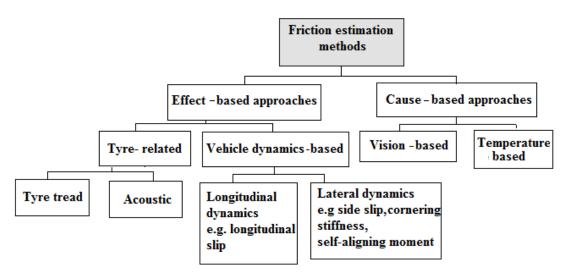
Figure 9. Classification of friction estimation methods

Vehicle dynamics-based methods exhibit more robustness to disturbances when compared to other methods. Lex [24] presented a detailed discussion of vehicle dynamics-based approaches to estimate the friction coefficient using mathematical and physical information.

As already discussed, accurate calculation of slip is essential for friction estimation and effective ABS control. From (4), it is evident that no matter what algorithm is used, true vehicle velocity v is always the basis for the calculation of slip. The wheel angular velocity can be accurately and easily measured by a wheel speed sensor. Though there are methods to measure vehicle velocity directly, they are often expensive and require additional wiring. This makes the system more complex and the inclusion of additional sensors may result in an increased need to mitigate sensor failures. An alternative is to estimate the vehicle velocity from existing information, particularly wheel velocity measurements. There are number of contributions focused on vehicle velocity estimation [26] [27] [28] [29]. Bowman [26] investigated measuring vehicle velocity based on using four accelerometer measurements or a combination of measurements from the wheel steering angle sensor and yaw rate sensor.

Jiang [30] presented an adaptive nonlinear filter to estimate vehicle velocity in order to calculate slip based on wheel velocity measurements only. This adaptive method is based on wheel speed and knowledge of the ABS operation. It is shown that the wheel speed periodically reflects the actual vehicle velocity.

Kun [31] and Melika [32] presented Kalman filter-based velocity estimation methods. These methods produce more accurate estimation and converge to the actual velocity but induce high transient errors. Melika [32] presented a new approach for velocity estimation combining a Kalman filter and adaptive estimation via data fusion to achieve more accurate estimation by eliminating the drawbacks of each approach when deployed in isolation. Belvy [7] estimated the vehicle velocity by utilizing GPS measurements. However, these methods also exhibit drawbacks in that the data fusion may require more time to process depending on the fusion architecture.

Kalman filter and fuzzy logic-based slip estimation methods were discussed by Bowman [26], Kobayashi [28] and Daiss [33]. Kobayashi [28] used a Kalman filter based on using wheel velocity and wheel acceleration signals. The derivative of wheel acceleration is assumed as a random noise signal and fuzzy logic is used to adjust the parameters of a Kalman filter.

Experiments were conducted on an actual vehicle and the results show good estimation of absolute vehicle velocity even under significant braking skid and track slip conditions. Ivanov [20] discussed cascaded fuzzy observers for evaluation of tyre-road interaction parameters. The work focused on identification of rolling resistance and friction parameters of a rolling wheel on both road and deformable surfaces.

Daiss [33] presented a fuzzy logic estimator which treats the vehicle velocity as a weighted sum of the measured wheel speed based on wheel speed sensor measurements and the vehicle acceleration. There is no model used and vehicle velocity, yaw rate and acceleration are estimated. Ray [29] presented an extended Kalman filter to estimate the vehicle velocity and tyre force. A nine degree of freedom model of the vehicle and tyre dynamics is used. The simulation results show that filtering can be achieved to provide state estimates for feedback control.

Dieckmann [34] investigated the relationship between slip and maximum friction coefficient where it was empirically proved that for the higher maximum friction coefficient the amount of slip required to produce a certain longitudinal tyre force is small within a low-slip ratio region. This is very useful when the friction coefficient is estimated in the low longitudinal slip region. Calculation of micro-slip, $\lambda < 0.1\%$, was explored using wheel speed sensor data only.

Uchanski [23] demonstrated that the variation in velocity must be slow to compute the difference between front and rear wheel speed over several revolutions. The major drawback is the presence of noise and uncertainties. Another disadvantage of this method is that the excitation level must be low for the method to be effective. A method to identify low-friction surfaces based on longitudinal vehicle velocity, ABS sensors and wheel speed sensors was also developed. The results show a strong correlation between the maximum coefficient of friction and low slip values. The major drawback is that the method depends on accurate estimation of slip and this is not possible using only measurements from the wheel speed sensor.

Gustafsson [35] investigated the problem encountered by Uchanski [23] when using the difference in wheel speed between the front and rear axles over a number of wheel revolutions. A linear relationship between the initial slip slope and desired coefficient of friction was used. A Kalman filter was used including a measurement offset of wheel speed that is estimated at the same time as the initial slip slope and the longitudinal slip. A drawback of this method is that it depends on prior knowledge of the maximum friction coefficient at the initial slope [34].

Ray [36] used an adaptive particle filter to estimate the maximum friction coefficient. This is a model-based approach where the effectiveness depends on the accuracy of the tyre and vehicle models used. The relationship between the maximum friction coefficient and both the longitudinal and lateral tyre forces was used. The major drawback is that such a particle filter contains internal states which cannot be measured directly.

Boßdorf-Zimmer [37] used an EKF to estimate the maximum friction coefficient and side slip angle based on a half-vehicle model and a nonlinear tyre model. The different levels of influence of the side slip angle and maximum friction coefficient on the lateral tyre force were combined.

3.4. Sliding mode observer design for estimation of friction coefficient and vehicle velocity

Sliding mode techniques have received wide application in problems relating to vehicle to dynamics as seen in the monographs [66] and [67]. A sliding mode observer based on the LuGre tyre model to estimate the friction coefficient was proposed in [38]. The observer uses wheel speed and brake pressure as measurements. The designed observers are then compared with an adaptive observer based on the parameter friction model developed by Yi [39]. The major drawbacks are the assumption that the vehicle and friction model parameters are fixed, that the proposed scheme is based on a quarter car model and considered only longitudinal velocity and slip which is not the case in reality and the effect of unmodelled dynamics is not considered. Further, no experimental validation is performed.

Patel [40] [41] and [42] proposed a SM based observer scheme to estimate the friction coefficient which is independent of the friction model. The performance of the observer is tested with the LuGre dynamic friction model. Tests indicate that the observer exhibits comparable performance with varying road conditions. However, only flat road driving conditions are tested.

A sliding mode observer is proposed in [43] and [44] to estimate the friction coefficient and vehicle velocity together. The method estimates the vehicle acceleration so that it can be used as an input for existing estimation algorithms of vehicle velocity and friction coefficient. The major drawback of this design is that it is based on a very simple friction model and the direct integration of the vehicle acceleration with experimental data cannot be performed in the presence of measurement noise. Experimental validation of the proposed scheme exhibited satisfactory performance on high and low grip road surfaces but performance during split-μ conditions was not satisfactory.

Sridi [47] [70] used sliding mode observers to estimate the tyre forces, vehicle velocity, wheel slip and tyre stiffness. The major drawback is that it uses a very simple linear relationship between the tyre force and friction coefficient and no experimental validation is reported. Furthermore, the road is assumed to be flat and any variation in the tyre forces is assumed to be slow.

Imine [60] [61] proposed a higher order sliding mode observer to estimate vertical tyre forces of a heavy vehicle. The estimated vertical tyre forces are then used to compute the Load Transfer Ratio (LTR) to prevent roll over risk [63] [64]. The proposed method is validated on an instrumented tractor. The innfluence of road profile inputs on the estimation of vertical forces for a heavy vehicle is explored in [62] [65]. Estimation of friction and vehicle parameters based on second order sliding mode methods is presented in [48]. In general, the vertical force is assumed to be constant for estimation of the friction coefficient for light vehicles but, in reality this is not always true. Hence, this strategy could be adapted or incorporated with other estimated tyre-forces (lateral and longitudinal) to improve the estimation of the friction coefficient.

Rajamani [49] [50] proposed a nonlinear observer to estimate vehicle longitudinal velocity by combining measurements from the wheel speed sensor and accelerometer to estimate longitudinal velocity. Though the estimation method considered the aerodynamic drag and uneven road conditions (climbing resistance), it exhibited under-damped estimation dynamics which is problematic for implementation.

Imsland [51] also proposed a nonlinear observer to estimate both the longitudinal and lateral

velocities of the vehicle. The longitudinal velocity is estimated based on wheel speed and longitudinal vehicle acceleration and the lateral velocity is estimated based on lateral vehicle acceleration and steering angle as inputs. A half-track vehicle model is used to describe the horizontal dynamics of the vehicle. Experimental results are presented but the results are only for circular manoeuvres which limit the performance assessment during normal driving conditions. The observer also exhibits poor performance on low μ surfaces.

Tannoury [52] proposed a higher order sliding mode observer scheme to estimate vehicle velocity based on wheel speed and brake torque measurements. The key feature of this design is that it considers the effective tyre radius for vehicle velocity estimation. Only constant vehicle speed and slowly varying speed are considered, and the model parameters are assumed to be constant.

Tanelli [53] presented a first order SMO to estimate vehicle velocity and road friction. The vehicle acceleration is estimated based on the low frequency component of the error dynamics of the observer and a measurement of wheel speed. Friction is estimated based on this estimated vehicle acceleration and vertical load. The scheme produces good results with experimental testing on a dry asphalt road but the effectiveness of the scheme is not validated for driving on a slope or switching between surfaces. The major issue with the scheme is that the influence of the suspension dynamics on the vehicle dynamics is not considered.

Tafner [54] discussed using a HSMO to estimate the lateral tyre force and cornering stiffness. The estimation scheme is two-stage and the observers are second order unknown input sliding mode observers. First, the lateral tyre forces are estimated using yaw rate measurements and this is then used to estimate the maximum lateral tyre forces. The lateral tyre force estimation is improved further by estimating and updating the cornering stiffness. The major concern is that the design only considers driving at constant vehicle speed.

Regolin [55] presented a cascaded sub-optimal second order sliding mode observer to estimate longitudinal and lateral forces based on single-track and single-wheel models. The key feature of this scheme is that it is not based on a specific tyre-road contact model. Simulation results with IPG-carmaker exhibit good performance for steering and longitudinal braking scenarios. The drawbacks of this scheme are that it is only valid under the assumption of no load transfer and its effectiveness in the presence of road profile changes and vertical load variation is not considered.

To summarise the identified gaps, there is no work reported considering the effect of the wheel dynamics, suspension dynamics and vehicle dynamics. For effective braking or traction control on diverse road conditions, precise estimation of slip and friction is required at this systems level. The influence of the wheel dynamics, suspension dynamics and vehicle dynamics are illustrated in Figure 10. In this paper SMO and HSMO schemes are presented to estimate slip and friction which consider all three dynamics. The SMO is designed to focus only on the linear relationship between slip and friction whereas the HSMO considers nonlinearity directly within the design.
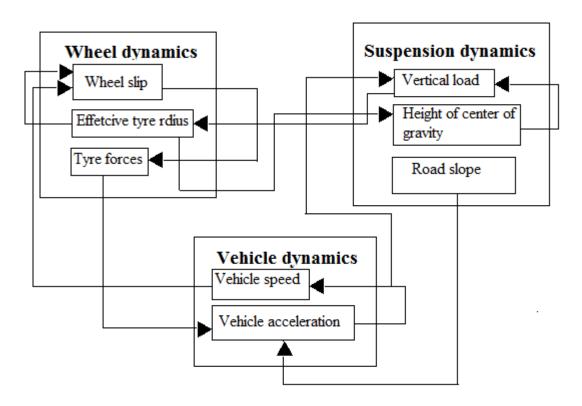
Figure 10. Illustration of coupling between all three system dynamics

4. SLIDING MODE OBSERVER DESIGN

In this section two estimation schemes based on the SM technique are designed to estimate vehicle velocity, slip and friction of a hybrid EV. The experimental vehicle used is a Delta E4 Coupe with two traction Electric Motors (EMs) that have been re-purposed to facilitate braking and slip control. First, a SMO scheme is designed based on a single-track model considering a linear relationship between wheel slip and friction to estimate slip and friction. Estimated vehicle velocity and effective tyre radius are used to estimate the slip. A HSMO is also designed to estimate vehicle velocity, frictional force, vertical force and then slip including tyre effective radius as a function of vertical force, considering the nonlinear relationship between wheel slip and friction.

4.1 Experimental vehicle, models, sensors and brake force requirements

The vehicle is a unique hybrid EV with electric brakes only on the rear drive wheel and friction brakes on the front. Two identical electric motors at the rear axle are modelled using a combination of a torque map, as supplied by the manufacturer, and a first order delay. The vehicle is installed with wheel speed sensors, torques sensors, suspension deflection sensors and a 6-Degree Inertial Measurement Unit (6D-IMU) which is a combination of angular rate sensors and an accelerometer to provide wheel speed, brake torque, acceleration and rotational rates respectively. The experimental vehicle is illustrated in Figure 11.

A hybrid force distribution strategy of ECE and ideal distribution curves shown in Figure 12 were selected for this unique braking configuration whereby at the highest deceleration (1g) the friction limit of the rear axle is exceeded. This will define the maximum force the rear axle is required to produce. Based on the above brake force distribution, to achieve 1g deceleration when braking from 100km/h, the rear axle needs to apply up to 4567 N through

the road.

Figure 11. Experimental vehicle

The vehicle is expected to achieve a maximum of 1g deceleration during braking and the so called 'time to lock' for a modern brake-by-wire system is estimated to be between 120 and 170 ms. Therefore the electric machines will ideally reach full torque less than 120 ms following the demand. The range of force distributions for decelerations of 0.2g $< a <$ 1.0g, is given in Figure 12a.
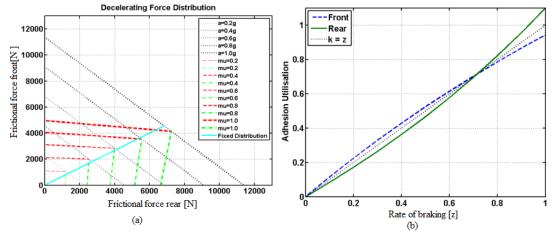

Figure 12. Brake force distribution between front and rear axles

The two electric machines on the rear axle each have a peak torque of 685 Nm and a rolling radius of 0.3m. This equates to a peak rear axle decelerating force of 4567 N. From the graph of adhesion utilisation against rate of braking (deceleration/g) in the Figure 12b, it can be seen that the rear wheels will lock when the friction coefficient $\mu > 0.7$. The motor torque limits are calculated based on the maximum regenerative power with respect to the State of Charge (SoC) of the battery pack. The results of experiments to determine appropriate limits based on the need to avoid damage to the battery are also used to inform the limits. Hence, a hybrid torque distribution scheme results.

Full car model

Figure 13 shows the full-vehicle model which consists of the horizontal model, vertical model, and tyre model. The heave, pitch and roll motions of the vehicle body are included. The lateral and longitudinal velocities of the vehicle (v_x and v_y, respectively) and the yaw rate constitute the four DOF related to the vehicle body at the centre of gravity (cg). This model obtains the longitudinal and lateral tyre forces from the tyre model. Based on these two forces, the horizontal model calculates the horizontal performance of the vehicle. The vertical model of

a vehicle contributes seven DOF and with an additional four DOF from the four wheels. This is depicted in Figure 13. This model is used primarily for testing.
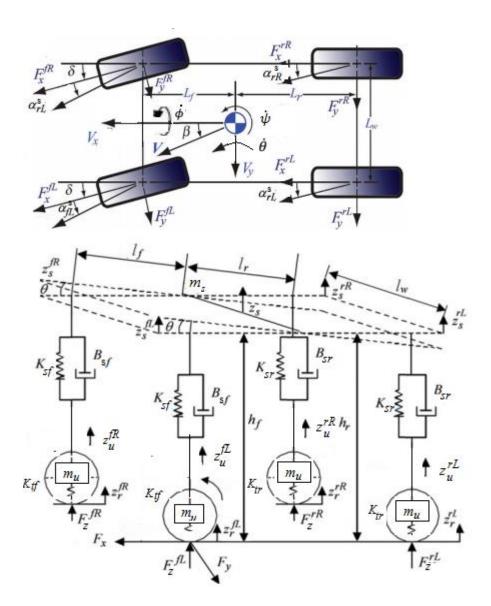

Figure 13. Full car model

The heave, pitch, roll and yaw motions of the vehicle body are included. The yaw, pitch and roll rates are denoted by $\dot{\psi}, \dot{\theta}, \dot{\phi}$, respectively and δ is the front wheel steering angle. The lengths L_f and L_r refer to the longitudinal distance from the cg to the front wheels and to the rear wheels, respectively, and L_w is the track width. Let the longitudinal and lateral tyre forces be given by F_x^{ij} and F_y^{ij}, respectively. The superscript or subscript i takes values f or r to indicate the front or rear of the vehicle, while the superscript or subscript j takes values L or R to indicate the left or right tyres, respectively.

Let z_s and z_s^{ij} denote the vertical displacement of the body at the centre and the corner, respectively, z_r^{ij} defines the road profile, θ is the body pitch angle, m_s is the sprung mass and

m_u^{ij} is the unsprung mass, F_z is the normal tyre force, and h_i is the vertical distance from the CoG to the centre of the front and the rear wheel at equilibrium. The spring and damping constants K_i and B_i, respectively, are the parameters associated with the sprung mass of the suspension system and K_{ti} is the unsprung mass constant.

The vehicle dynamics can be represented by:

$$\ddot{\psi} = \frac{1}{I_\psi}\Big[L_f\big(F_x^{fL} + F_x^{fR}\big)\sin\delta - L_f\big(F_y^{fL} + F_y^{fR}\big)\cos\delta \tag{10}$$

$$+ L_f\big(F_x^{fL} + F_x^{fR}\big)\Big]\Big[\frac{L_w}{2}\big(F_x^{fL} - F_x^{fR}\big)\cos\delta - \frac{L_w}{2}\big(F_y^{fL} - F_y^{fR}\big)$$

$$+ \frac{L_w}{2}\big(F_x^{fL} - F_x^{fR}\big)\sin\delta\Big]$$

$$\ddot{z}_s = \frac{1}{m_s}\Big[mg - K_{sf}z_s^{fL} - B_{sf}\dot{z}_s^{fL} - K_{sf}z_s^{fR} - B_{sf}\dot{z}_s^{fR}\Big] \tag{11}$$

$$- \Big[K_{sr}z_s^{rL} - B_{sr}\dot{z}_s^{rL} - K_{sr}z_s^{rR} - B_{sr}\dot{z}_s^{rR}\Big]$$

$$\ddot{\theta} = \frac{h_f}{I_\theta}\big(F_x^{fL} + F_x^{fR}\big)\cos\delta + \big(F_y^{fL} + F_y^{fR}\big)\sin\delta - h_r\big(F_x^{fL} + F_x^{fR}\big) \tag{12}$$

$$- L_f\big(K_{sf}z_s^{fL} + B_{sf}\dot{z}_s^{fL} + K_{sf}z_s^{fR} + B_{sf}\dot{z}_s^{fR}\big)$$

$$+ L_r\big(K_{sr}z_s^{rL} - B_{sr}\dot{z}_s^{rL} - K_{sr}z_s^{rR} - B_{sr}\dot{z}_s^{rR}\big)$$

$$\ddot{\phi} = \big(F_y^{fL} - F_y^{fR}\big)\sin\delta + \big(F_x^{fL} - F_x^{fR}\big)\cos\delta + h_r\big(F_x^{rR} - F_x^{rL}\big) \tag{13}$$

$$- \frac{L_w}{2}\big(K_{sf}z_s^{fR} + B_{sf}\dot{z}_s^{fR} + K_{sr}z_s^{rR} + B_{sr}\dot{z}_s^{rR}\big)$$

$$- \frac{L_w}{2}\big(K_{sf}z_s^{fL} + B_{sf}\dot{z}_s^{fL} + K_{sr}z_s^{rL} + B_{sr}\dot{z}_s^{rL}\big)$$

$$\dot{v}_y = \frac{1}{m}\Big[\big(F_y^{fL} + F_x^{fR}\big)\cos\delta + \big(F_x^{fL} + F_x^{fR}\big)\sin\delta + \big(F_x^{fL} + F_x^{fR}\big) - \dot{\psi}v_y\Big] \tag{14}$$

$$\dot{v}_x = \frac{1}{m}\Big[\big(F_x^{fL} + F_x^{fR}\big)\cos\delta - \big(F_y^{fL} + F_y^{fR}\big)\sin\delta + \big(F_x^{fL} + F_x^{fR}\big) + \dot{\psi}v_x\Big] \tag{15}$$

where

$$z_s^{fL} = z_s - z_u^{fL} + L_f\theta + L_w\,\phi/2\,, z_s^{fR} = z_s - z_u^{fR} + L_f\theta - I_w\,\phi/2,$$

$$z_s^{rL} = z_s - z_u^{rL} - L_f\theta + L_w\,\phi/2, z_s^{rR} = z_s - z_u^{rR} - L_f\theta - I_w\,\phi/2,$$

$$\dot{z}_s^{fL} = \dot{z}_s - \dot{z}_u^{fL} + L_f\dot{\theta} + L_w/2\,\dot{\phi}, \dot{z}_s^{fR} = \dot{z}_s - \dot{z}_u^{fR} + L_f\dot{\theta} - L_w/2\,\dot{\phi},$$

$$\dot{z}_s^{rL} = \dot{z}_s - \dot{z}_u^{rL} - L_f\dot{\theta} + L_w/2\,\dot{\phi}, \dot{z}_s^{rR} = \dot{z}_s - \dot{z}_u^{rR} - L_f\dot{\theta} - L_w/2\,\dot{\phi}$$

$$m_u\ddot{z}_u^{ij} = -b_s\big(\dot{z}_u^{ij} - \dot{z}_s^{ij}\big) - k_s\big(z_u^{ij} - z_s^{ij}\big) - K_{ti}\big(z_u^{ij} - z_r^{ij}\big)$$

Single- track vehicle model

In this model, which is used to develop the SMO, only the vehicle longitudinal motion is considered as shown in Figure 14. When the vehicle is experiencing deceleration, the vehicle longitudinal dynamics model and wheel dynamics model can be described as:

$$\dot{v} = \frac{1}{m}\left(F_{xr} + F_{xf}\right) - C_r g - \frac{D_a v^2}{m} + g\sin\theta_s \qquad (16a)$$

$$\dot{\omega}_r = \frac{1}{I_\omega}\left(-F_{xr}R + T_{br}\right) \qquad (16b)$$

$$\dot{\omega}_f = \frac{1}{I_\omega}\left(-F_{xf}R + T_{bf}\right) \qquad (16c)$$

$$F_{zf} = \frac{m}{2(L_f + L_r)}\left(gL_f - ha_x\right) \qquad (16d)$$

$$F_{zr} = \frac{m}{2(L_f + L_r)}\left(gL_r + ha_x\right) \qquad (16e)$$

where the rolling resistance $C_r mg$, wind drag force $D_a v^2$ and road gradient θ_s are considered. T_{bf} and T_{br} are the braking torques applied to the front and rear wheels respectively.
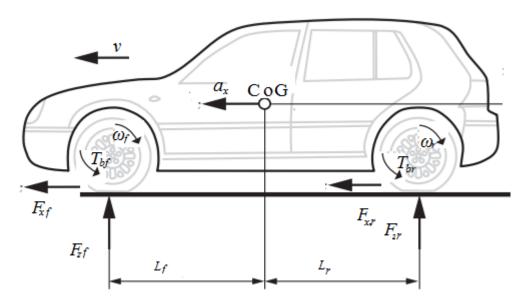
Figure 14. Single-track vehicle model

The ω_f and ω_r are the angular speeds of the front and rear wheels respectively and a_x is the acceleration of the vehicle. The vehicle mass is denoted m, I_ω is the moment of inertia of the wheel and R is the tyre radius.

Effective radius of the tyre

Hirschberg [71] states that the effective radius, illustrated in Figure 15. is given by $R_e = C_e /2\pi$, where C_e is the effective rolling circumference. Both R_e and C_e depend on the vertical force F_z and wheel speed ω.
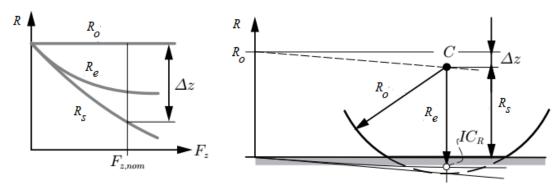
Figure 15. Tyre-effective radius (adopted from [8])

where R_s and R_o are the static tyre radius and free rolling radius, IC_R is the instantaneous tyre centre and unloaded tyre radius respectively and Δz_v describes the influence of the vertical force F_z in the tyre vertical deflection. The approximate effective tyre radius is given by

$$R_e = \frac{1}{3}R_0 + \frac{2}{3}R_s = R_0 - \frac{2}{3}\Delta z_v \tag{17a}$$

$$R_e \approx R_0 - \frac{2}{3}\frac{F_z}{C_s} \tag{17b}$$

where $\Delta z_v \approx \frac{F_z}{C_s}$ and C_s is the linear static tyre stiffness at the operating point.

4.2. SMO Scheme

A cascaded observer structure (see Figure 16) is used to estimate the slip and friction coefficient based on a linear relationship of $\mu - \lambda$. First, vehicle velocity is estimated based on road slope calculation assuming small slip. Then estimated vehicle acceleration is used to estimate vertical force which is used to estimate effective tyre radius. Slip is estimated using estimated effective tyre radius and vehicle velocity.
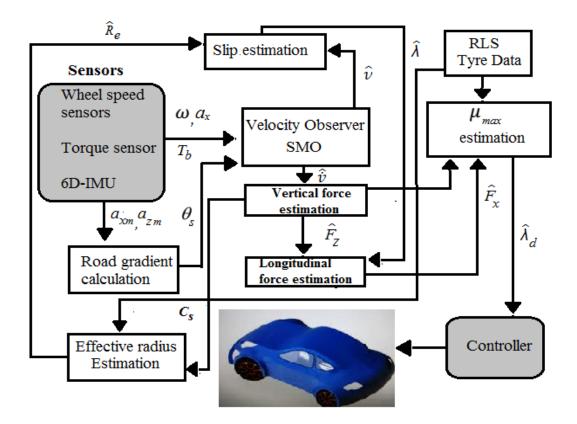
Figure 16. SMO scheme

Then the estimated slip and longitudinal deceleration are used to estimate the longitudinal tyre force and the C_s, the tyre stiffness is assumed constant in the linear region. Finally, the friction coefficient is estimated.

The velocity of the vehicle is re-written in terms of the angular speed of the wheels and torques from (16) to obtain

$$\dot{v} = \frac{-(T_{bf} + T_{br}) - I_\omega(\omega_f + \omega_r)}{mR} - C_r g - \frac{D_a v^2}{m} + g \sin\theta_s \qquad (18)$$

Before the observer is designed the following assumption is made,

Assumption 1: *The lateral motion of the vehicle is neglected and the road gradient θ_s is constant. The wheel angular speed ω, brake torque T_b and longitudinal deceleration a_x are measurable. The effective tyre radius is estimated using (17b) based on estimated vertical force.*

Remark 1: *The wheel speed can be measured by the installed wheel speed sensors and the road gradient can be calculated using the 6D-IMU and wheel speed sensors assuming slip is small. The brake torque and the longitudinal deceleration are obtained by the torque sensor and 6D-IMU, respectively. The relationship between μ and λ is assumed to be linear even in the low slip range. Hence, the calculation of effective tyre radius using (17) is valid and the assumptions are reasonable.*

The observer is designed based on the dynamics given in (18), as follows:

$$\dot{\hat{v}} = \frac{-(T_{bf} + T_{br})}{mR} \cdot L(\hat{v} - r\omega_f) - \frac{I_\omega(\dot{\omega}_f + \dot{\omega}_r)}{mR} - C_r g - \frac{D_a \hat{v}^2}{m}$$
$$+ g\sin\theta_s + K\left[\frac{(T_{bf} + T_{br})}{mR} \cdot L(\hat{v} - r\omega_f) - \frac{I(\dot{\omega}_f + \dot{\omega}_r)}{mR}\right.$$
$$\left. - C_r g - a_x\right] \tag{19}$$

Remark 2: The observer input signals are T_{bf}, T_{br}, ω_f and ω_r. These are calculated from the torque sensor and wheel speed sensors respectively. The linear acceleration a_x is measured by the 6D-IMU and used as feedback to the observer to allow it to converge with the designed feedback gain K. L is defined as

$$L(s) = \begin{cases} -1, & s > n \\ 1, & s < n \\ \dfrac{s}{n}, & \text{else} \end{cases} \tag{20}$$

where $s = \hat{v} - R\omega_f$ and n is 0.1. This boundary layer alleviates the chattering problem. By defining the estimation error $\tilde{v} = v - \hat{v}$, the error dynamics can be obtained by (18) - (19) as follows

$$\tilde{v} = \left(\frac{T_{bf} + T_{br}}{mR}\right)(-1 - L(s)) - \frac{D_a(v^2 - \hat{v}^2)}{m}$$
$$- K\left[\left(\frac{T_{bf} + T_{br}}{mR}\right)L(s) - \frac{I_\omega(\dot{\omega}_f + \dot{\omega}_r)}{mR} - C_r g - \frac{D_a \hat{v}^2}{m}\right.$$
$$\left. - a_x\right] \tag{21}$$

where the deceleration $a_x = \frac{-(T_{bf}+T_{br})-I_\omega(\dot{\omega}_f+\dot{\omega}_r)}{mR_e} - C_r g - \frac{D_a\widehat{v^2}}{m}$ is measured using the longitudinal accelerometer and used as feedback to the observer. Thus, the error dynamics from (21) can be re-arranged as follows

$$\dot{\tilde{v}} = \frac{(T_{bf} + T_{br})}{mR}(L(s) + 1) - (1 + K)\frac{D_a(v + \hat{v})}{m}$$
$$- K\left[\frac{(T_{bf} + T_{br})}{mR}(L(s) + 1)\right]\hat{v} \tag{22}$$

Hence, with the condition $K > 0$, it follows that $L(s) \rightarrow -1, \tilde{v} \rightarrow 0$ during vehicle deceleration and if there is an increase in vehicle velocity then, $L(s) \rightarrow 1$, and $\tilde{v} \rightarrow 0$. Therefore, the designed observer (19) can ensure accurate, stable estimation of vehicle velocity under the conditions of *Assumption 1.*

Road slope calculation

Road slope can be calculated using measurements (6D-IMU) and, assuming the vehicle is moving in a straight line, slip is small, and the road slope is constant. An illustration is given below in Figure 17.
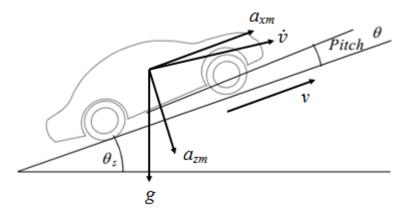
Figure 17. Road slope calculation

The measurement from the vertical accelerometer can be expressed as

$$a_{zm} = a_z + g\cos(\theta_s + \theta) \tag{23}$$

$$a_z = \frac{d\omega_v}{dt}\sin\theta \tag{24}$$

$$a_{zm} = \frac{d\omega_v}{dt}\sin\theta + g\cos(\theta_s + \theta) \tag{25}$$

where a_z is the component of the vehicle acceleration in the z-direction and ω_v is the wheel speed. Similarly, considering the longitudinal sensors yields

$$a_{xm} = a_x - g\sin(\theta_s + \theta) \tag{26}$$

$$a_x = \frac{d\omega_v}{dt}\cos\theta \tag{27}$$

$$a_{xm} = \frac{d\omega_v}{dt}\cos\theta - g\sin(\theta_s + \theta) \tag{28}$$

From equations (25) and (28):

$$a_{xm}^2 + a_{zm}^2 = g^2 + \frac{d^2\omega_v}{dt} - 2g\frac{d\omega_v}{dt}\sin\theta_s \tag{29}$$

For a small road slope angle, equation (29) can be re-arranged to estimate the road slope as follows

$$\theta_s = \frac{\left(a_{xm}^2 + a_{zm}^2 - g^2 - \frac{d\omega^2}{dt}\right)}{2g\frac{d\omega_v}{dt}} \tag{30}$$

Tyre force estimation

The wheel slip is then calculated using the estimated vehicle velocity, wheel angular speed and estimated effective tyre radius using (17) based on estimated vertical force.

Assumption 2: *The lateral tyre force is neglected and the tyre stiffness is unique for a road surface.*
Remark 3: *The slip calculation using estimated vehicle velocity and approximate effective tyre radius given in (17b) is valid where there is a linear relationship between μ and λ.*

The tyre forces are estimated as follows:

$$\hat{F}_x = \hat{F}_{xf} + \hat{F}_{xr} = \Omega \hat{\lambda}_f + \Omega \hat{\lambda}_r \tag{31}$$

$$\hat{F}_{zf} = \frac{m}{2(L_f + L_r)}\left(gL_f - h\hat{v}\right) \tag{32}$$

$$\hat{F}_{zr} = \frac{m}{2(L_f + L_r)}\left(gL_r + h\hat{v}\right) \tag{33}$$

where

$$\hat{\lambda}_f = \frac{\hat{v} - \hat{R}_e \omega_f}{\hat{v}} \quad \text{and} \quad \hat{\lambda}_r = \frac{\hat{v} - \hat{R}_e \omega_r}{\hat{v}}$$

where Ω is a ratio which defines the relationship between longitudinal tyre force and longitudinal slip. In the linear region, $\Omega = C_s$, but it should be updated when the relationship becomes nonlinear. Hence, a design parameter G is introduced to adjust Ω with respect to the variation in the tyre force estimation error e.

$$\Omega = Ge - C_s \tag{34}$$

μ-λ curve fitting

The estimate of the road friction coefficient μ can be expressed as follows:

$$\hat{\mu} = \frac{\hat{F}_x}{\hat{F}_z} = C_s \hat{\lambda} \tag{35}$$

Remark 4: *The longitudinal tyre stiffness C_s is dependent on the road surface.*

The Recursive Least Square (RLS) method [35] is used to obtain C_s using experimental tyre data to estimate the μ, and the estimation steps are given by

$$\hat{C}_s(t) = \hat{C}_s(t-1) + K_{rls}(t)\left[\frac{\hat{F}_x(t)}{\hat{F}_z(t)} - \hat{C}_s(t-1)\lambda(t)\right] \tag{36}$$

$$K_{rls}(t) = \frac{P(t-1)\lambda(t)}{\beta_f + P(t-1)\lambda^2(t)} \tag{37}$$

$$p(t) = \frac{1}{\beta_f}\left[p(t-1) - \frac{P^2(t-1)\lambda(t)}{\beta_f + P(t-1)\lambda^2}(t)\right] \tag{38}$$

where $K_{rls}(t)$ is the update gain, $P(t)$ the error covariance and β_f the forgetting factor. The obtained C_s is used to estimate the maximum coefficient of friction and the methodology is illustrated in Figure 18.
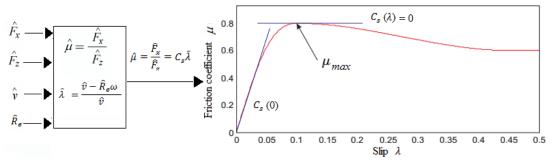

Figure 18. μ-λ curve fitting using C_s

4.3 HSMO Scheme

An adaptive HSMO is now designed to estimate vehicle velocity, road slope, tyre force and slip. First, an adaptive HSMO is designed based on the quarter car model to estimate the vehicle velocity at the front wheels. It considers all nonlinear relationship between the slip and friction. The influencing factors of all three systems: wheel, suspension and vehicle dynamics are estimated. Then, the obtained vehicle acceleration and road slope are used to estimate the vertical tyre force and friction force. This improves the estimate of vertical force when compared to the estimate obtained using the SMO (19) designed in Section 4.2. The SMO scheme only considers simple load transfer and full suspension dynamics are not considered. Furthermore, the SMO scheme calculates road slope based on small slip and assumes it to be constant. Effective tyre radius is also estimated using (17a) directly considering Δz_v based on CoG shift. The estimation scheme is shown schematically in Figure 19.
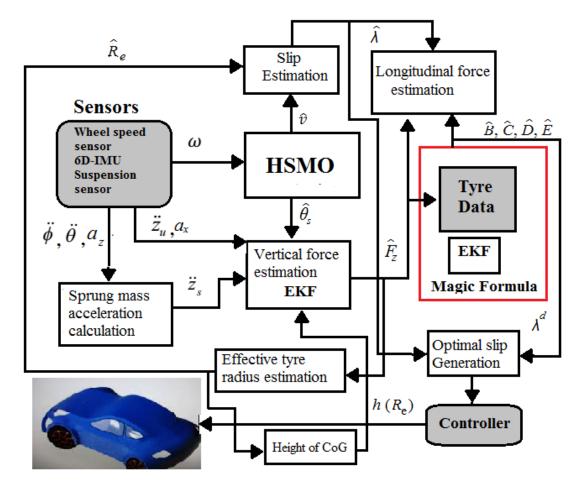
Figure 19. HSMO scheme

Velocity estimation

The observer design is based on the super-twisting algorithm discussed by Levant [56] and uses only wheel speed measurements. The quarter car model described in equations (1), (2) and (3) is improved by including the approximate tyre effective radius, aerodynamic drag, road gradient and rolling resistance. The dynamic equations are given below.

$$I_\omega \dot{\omega} = R_e F_x - T_b \tag{39}$$

$$m\dot{v} = F_x - F_d - F_r + g \sin \theta_s \tag{40}$$

$$F_d = \frac{1}{2}\rho_d A C_d v^2 = D_a v^2 \text{ and } F_r = mgC_r \tag{41}$$

where F_d is the aerodynamic drag force, F_r is the rolling resistance force, C_d and C_r are the coefficients of aerodynamic drag and rolling resistance. The mass density of air is ρ_d, the frontal area of the vehicle is A and D_a is the lumped air drag term.

Estimation of vehicle velocity is highly influenced by uncertainties due to unevenness of the road, the friction coefficient of the surface and the variation in the frictional force. The work reported in the literature such as [32] [43] [53] [57] assumes the frictional coefficient is constant and the corresponding frictional force is available for estimation of vehicle velocity.

Hence, to improve estimation, an Adaptive Higher Order Sliding Mode Observer (AHSMO) is designed which considers the uncertainties due to road gradient and frictional coefficient as well as the possible influence of neglected dynamics (e.g suspension) which are treated as disturbances to the system. An AHSMO is designed to estimate and offset the influence of uncertainties and the disturbance.

Remark 5: *The gradient of the road, or the slope, influences the vehicle deceleration and hence, the tyre forces. The acceleration measurements provided by the accelerometer (IMU) represent the combined acceleration due to gravity and frictional force. Therefore, variation in road slope due to irregularities (bumps) and changes in the frictional coefficient are considered in the estimation as uncertainties, Δf. Furthermore, an external disturbance d is also added to the system to characterize unknown factors/neglected dynamics (e.g lateral dynamics and suspension dynamics) that influence deceleration.*

Assumption 3: *The road gradient is assumed to be small, hence, $g \sin \theta_s \approx g\theta_s$. The rate of change in road slope is given as $\dot{\theta}_s = q$, and is assumed to be unknown and small.*

The state space representation of the system is given by

$$\dot{x}_i = f_i(x) + \Delta f_i + g_i(x)u + d_i \tag{42}$$

where i = 1, 2, 3, and

$$f(x) = \begin{bmatrix} \dfrac{-1}{I}\left(R_e F_x + C_f x_1\right) \\ \dfrac{1}{m}\left(F_x - F_d - F_r + g\theta_s\right) \\ q \end{bmatrix}, g(x) = \begin{bmatrix} \dfrac{1}{I} \\ 0 \\ 0 \end{bmatrix}$$

$$\Delta f = \begin{bmatrix} \Delta F_x \\ \Delta F_x \\ \Delta q \end{bmatrix}, d = \begin{bmatrix} d_1 \\ d_2 \\ 0 \end{bmatrix}, \ u = T_b \text{ and } x = [\omega, v, \theta_s]^T$$

ΔF_x and Δq represent the uncertainties in μ and q, respectively. Let $D = \Delta f + d$ to design the AHSMO.

Adaptive Higher Order Sliding Mode Observer (AHSMO)

An adaptive observer is designed based on the super-twisting algorithm presented by Levant [56], to estimate vehicle velocity by offsetting the influence of the uncertainties and disturbance. The Higher Order Sliding Mode (HOSM) alleviates the chattering problem of a conventional sliding mode scheme, and also retains the advantages of the latter in terms of robustness.

An Adaptive Higher Order Sliding Mode Observer (AHSMO) is constructed for each element of the state of the system (42) as

$$\begin{aligned} \sigma_i &= x_i - z_i \\ \dot{z}_i &= f_i(x) + g_i(x)u + \alpha_i \end{aligned} \tag{43}$$

where

$$\alpha_i = l_{i1} \cdot |\sigma_i|^{\frac{1}{2}} \cdot sign(\sigma_i) + l_{i2} \cdot \int sign(\sigma_i) dt \tag{44}$$

The adaptation law is given by

$$\dot{l}_{i1} = \rho_i \|x_i\| \, \|\sigma_i\| \tag{45}$$

where

$$l_{i2} = \frac{\varepsilon}{2l_{i1}} + \frac{1}{2}\varepsilon^2 + \frac{1}{2}\Gamma \tag{46}$$

Here, σ_i is the sliding surface, x_i is the state of the system, z_i is the state of the observer, α_i is the input of the assist control, ρ_i, ε and Γ are any positive number.

Theorem 1: If in equation (44) the parameter l_{il} satisfies $l_{i1} \geq (\varepsilon + \delta_i)(\Gamma + \varepsilon^2) + \frac{\varepsilon}{2}\frac{(\delta_i^2 + 1)}{\Gamma}$ and l_{i2} is chosen as in equation (46), then the sliding surface σ_i will converge to zero in finite time. It follows that an estimate of the disturbance, $\widehat{D}_i$, is then given by $\widehat{D}_i = \alpha_i$.

Proof: Differentiating equation (43):

$$\dot{\sigma}_i = \dot{x}_i + \dot{z}_i = f_i(x) + g_i(x)u + D_i - f_i(x) - g_i(x)u - \alpha_i = D_i - \alpha_i \tag{47}$$

which yields

$$\dot{\sigma}_i + \alpha_i = D_i$$

Substitute equation (44) into equation (47), and rearrange to obtain

$$\dot{\sigma}_i = -l_{i1} \cdot |\sigma_i|^{\frac{1}{2}} sign(\sigma_i) + \alpha_i + D_i \tag{48}$$
$$\dot{\alpha}_i = -l_{i2} sign(\sigma_i)$$

Let $\eta_i = \begin{bmatrix} \zeta_{i1} \\ \zeta_{i2} \end{bmatrix} = \begin{bmatrix} |\sigma_i|^{\frac{1}{2}} sign(\sigma_i) \\ \alpha_i \end{bmatrix}$, and according to equation (48), one can obtain:

$$\dot{\zeta}_{i1} = \frac{1}{2|\sigma_i|^{\frac{1}{2}}} (-l_{i1}\zeta_{i1} + \zeta_{i2} + D_i)$$

$$\dot{\zeta}_{i2} = -l_{i2} sign(\sigma_i) = -l_{i2}(\zeta_{i1}) = \frac{-1}{|\sigma_i|^{\frac{1}{2}}} l_{i2}\zeta_{i1} \tag{49}$$

That is

$$\dot{\zeta}_i = \frac{1}{|\sigma_i|^{\frac{1}{2}}} \begin{bmatrix} \frac{-l_{i1}}{2} & \frac{1}{2} \\ -l_{i2} & 0 \end{bmatrix} \zeta_i + \frac{1}{|\sigma_i|^{\frac{1}{2}}} \begin{bmatrix} \frac{1}{2} \\ 0 \end{bmatrix} D_i \tag{50}$$

and it can be re-written as

$$\dot{\zeta}_i = A_i \zeta_i + B_i D_i \tag{51}$$

where , $A_i = \dfrac{1}{|\sigma_i|^{\frac{1}{2}}}\begin{bmatrix} \dfrac{-l_{i1}}{2} & \dfrac{1}{2} \\ -l_{i2} & 0 \end{bmatrix}$, $B_i = \dfrac{1}{|\sigma_i|^{\frac{1}{2}}}\begin{bmatrix} \dfrac{1}{2} \\ 0 \end{bmatrix}$.

In fact, if ζ_{i1} and ζ_{i2} converge to zero in finite time, σ and $\dot{\sigma}$ also converge to zero in finite time.

The Lyapunov function is selected as [69]

$$V = \zeta_i^T P \zeta_i + \frac{1}{2k}\left(l_{i1} - \hat{l}_{i1}\right)^2 \tag{52}$$

where k is any positive value. Let $V_0 = \zeta_i^T P \zeta_i$, then equation (52) can be re-written as

$$V = V_0 + \frac{1}{2k}\left(l_{i1} - \hat{l}_{i1}\right)^2 \tag{53}$$

where $P = \begin{bmatrix} \Gamma + \varepsilon^2 & -\varepsilon \\ -\varepsilon & 1 \end{bmatrix}$, ε and Γ are any positive value. Therefore, P is a positive definite matrix.

The time derivative of V_0 is

$$\dot{V}_0 = \dot{\zeta}_i^T P \zeta_i + \zeta_i^T P \dot{\zeta}_i = \zeta_i^T\left(PA_i + A_i^T P\right)\zeta_i + 2D_i B_i^{TP}\zeta_i = \frac{-1}{|\sigma_i|^{\frac{1}{2}}}\zeta_i^T Q \zeta_i + 2D_i B_i^T P \zeta_i \tag{54}$$

According to equations (50) and (51), one can obtain

$$Q = \begin{bmatrix} l_{i1}(\Gamma + \varepsilon^2) - 2l_{i2}\varepsilon & l_{i2} - \frac{l_{i1}}{2}\varepsilon - \frac{1}{2}(\Gamma + \varepsilon^2) \\ 0 & \varepsilon \end{bmatrix} \tag{55}$$

$$2B_i^T P = -\frac{1}{|\sigma_i|^{\frac{1}{2}}}[\Gamma + \varepsilon^2 \quad -\varepsilon] \tag{56}$$

By letting $M = -[\Gamma + \varepsilon^2 \quad -\varepsilon]$, equation (54) can be re-written as

$$\dot{V}_0 = -\frac{1}{|\sigma_i|^{\frac{1}{2}}}\zeta_i^T Q \zeta_i - \frac{D_i}{|\sigma_i|^{\frac{1}{2}}}M\zeta_i \tag{57}$$

Let $\dot{V}_0 < -\dfrac{1}{|\sigma_i|^{\frac{1}{2}}}\zeta_i^T \tilde{Q}\zeta_i = -\dfrac{1}{|\sigma_i|^{\frac{1}{2}}}\zeta_i^T\left(Q + \hat{Q}\right)\zeta_i$, because if $|D_i| \leq \delta_i\left|\sigma_i\right|^{\frac{1}{2}}$, then

$$\hat{Q} = -\frac{1}{|\sigma_i|^{\frac{1}{2}}}\begin{bmatrix} -\delta_i(\Gamma + \varepsilon^2) & \frac{1}{2}\delta_i\varepsilon \\ 0 & 0 \end{bmatrix} \tag{58}$$

Hence,

$$\tilde{Q} = Q + \hat{Q} = \begin{bmatrix} (l_{i1} - \delta_i)(\Gamma + \varepsilon^2) - 2l_{i2}\varepsilon & l_{i2} - \frac{1}{2}\varepsilon l_{i1} - \frac{1}{2}(\Gamma + \varepsilon^2) + \frac{1}{2}\delta_i\varepsilon \\ 0 & \varepsilon \end{bmatrix} \tag{59}$$

Let $l_{i2} = \frac{1}{2}\varepsilon l_{i1} + \frac{1}{2}\varepsilon^2 + \frac{1}{2}\Gamma$ and substitute (58) into (59) to obtain

$$\tilde{Q} = \begin{bmatrix} l_{i1}\Gamma - (\varepsilon + \delta_i)(\Gamma + \varepsilon^2) & \frac{1}{2}\delta_i\varepsilon \\ 0 & \varepsilon \end{bmatrix} \tag{60}$$

Hence, if $l_{i1} \geq (\varepsilon + \delta_i)(\Gamma + \varepsilon^2) + \frac{\varepsilon}{2}\frac{(\delta_i^2+1)}{\Gamma}$, $\Gamma_{min}(\tilde{Q}) \geq \frac{\varepsilon}{2}$, then

$$\dot{V}_0 = -\frac{\Gamma_{min}(\tilde{Q})\Gamma_{min}^{\frac{1}{2}}(P)}{\Gamma_{max}(P)} V_0^{\frac{1}{2}} \tag{61}$$

Now let $\Pi = \frac{\Gamma_{min}(\tilde{Q})\Gamma_{min}^{\frac{1}{2}}(P)}{\Gamma_{max}(P)}$ to obtain

$$\dot{V} = \dot{V}_0 + \frac{1}{k}(l_{i1} - \hat{l}_{i1})\dot{l}_{i1} = -\Pi V_0^{\frac{1}{2}} + \frac{1}{k}(l_{i1} - \hat{l}_{i1})\dot{l}_{i1} < 0 \tag{62}$$

Therefore, for the adaptive higher order sliding mode observer (43) with α_i defined by (44), both σ_i and $\dot{\sigma}_i$ converge to zero in finite time.

The super -twisting based HSMO presented could be adapted and implemented to naval and aerospace problems [68]. For example, the proposed scheme could be adapted to develop observer-based adaptive control systems for underwater missiles.

Tyre force estimation

Unlike the SMO scheme, which assumes a linear relationship between frictional force and slip, the HSMO scheme updates the parameters of the magic formula. To estimate the frictional force, (7) is re-arranged to describe the influence of vertical force and slip on the parameters as follows

$$F_x = D_p\sin\left(C\tan^{-1}(B\phi)\right) \tag{63}$$

Where

$$\phi = (1 - E)\lambda + \left(\frac{E}{B}\right)\tan^{-1}(B\lambda) \qquad \lambda = \frac{v - \omega R_e}{v} \qquad R_e = R_o - \frac{2}{3}\frac{F_z}{C_s}$$

$$C = \rho_m c_{x1} \qquad\qquad D_p = \mu_x F_Z \qquad\qquad E = \rho_{m1} + \rho_{m2}df_z + \rho_{m3}df_z^2$$

$$B = F_z(\rho_{m1} + \rho_{m2}df_z)\exp(\rho_{m3}df_z)/(CD)$$

where $\rho_{m1,}\ \rho_{m2,}\ \rho_{m3}$ are vertical force dependant coefficients.

An integrated model of the vertical dynamics and longitudinal dynamics incorporating an improved suspension model is considered. During severe braking with a deceleration of 1g, which is a design point of interest for this study, the pitching and road slope effects are significant when the vertical force is estimated, hence, wheel-suspension-vehicle dynamic coupling should be analysed. Furthermore, the resulting shift in the CoG and associated variation in effective tyre radius is also considered.
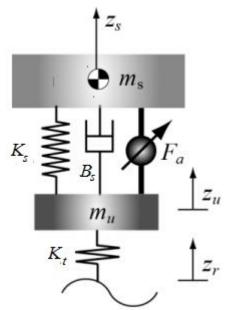
.

Figure 20. Suspension dynamics

The vertical force F_z, has two components: the force due to the longitudinal load transfer and the force due to the suspension dynamics, illustrated in Figure 20.

In this figure, m_s is the sprung mass, m_u is the unsprung mass, K_s is the spring stiffness, B_s is the damping constant, k_t is the unsprung constant, F_a is the controlled actuator force and z_s, z_u, z_r are the vertical displacements of sprung mass, unsprung mass and the displacement due to road irregularity respectively.

Remark 6: *The vertical forces described by (16d) and (16e) assume the deceleration a_x is measured by inertial sensors. In reality, the deceleration measured by IMU is affected by the road slope, roll and pitch of the vehicle. Hence the combined deceleration due to vehicle motion and gravity is expressed as: $a_x = \dot{v}\cos\theta + g\sin(\theta + \theta_s)$ where $\dot{v}$ and g are the deceleration due to vehicle motion and gravity respectively. θ, θ_s are the pitch and road slope, respectively. Assuming pitch and road slope are small and $\theta \ll \theta_s$, the deceleration $a_x = \dot{v} + g\theta_s$.*

The vertical force due to longitudinal load transfer is given by the following equations.

$$F_{zf} = (m_s + m_u)g - \frac{(m_s + m_u)(\dot{v} + g\theta_s)h_f}{2(L_f + L_r)}$$

$$F_{zr} = (m_s + m_u)g + \frac{(m_s + m_u)(\dot{v} + g\theta_s)h_r}{2(L_f + L_r)}$$

(64)

The vertical force due to the suspension dynamics is given by

$$F_{zd} = m_s\ddot{z}_s + m_u\ddot{z}_u \tag{65}$$

where

$$m_s\ddot{z}_s = -B_s(\dot{z}_s - \dot{z}_u) - K_s(z_s - z_u) \tag{66}$$

$$m_u\ddot{z}_u = -B_s(\dot{z}_u - \dot{z}_s) - K_s(z_u - z_z) - K_t(z_u - z_r) \tag{67}$$

$$\ddot{z}_s = z - L_{f/r} - \ddot{\theta} - L_w\ddot{\phi} \tag{68}$$

θ, ϕ are the pitch and roll angles respectively. L_w is the track width and $L_{f/r}$ is the distance between CoG to front/rear wheel center.

The total vertical force is given by

$$F_{zf} = (m_s + m_u)g - \frac{(m_s + m_u)(\dot{v} + g\theta_s)h_f}{2(L_f + L_r)} + m_s\ddot{z}_s + m_u\ddot{z}_u \tag{69}$$

$$F_{zr} = (m_s + m_u)g + \frac{(m_s + m_u)(\dot{v} + g\theta_s)h_r}{2(L_f + L_r)} + m_s\ddot{z}_s + m_u\ddot{z}_u$$

The vertical force is estimated using an Extended Kalman Filter (EKF).

Consider the following nonlinear discrete-time system:

$$x_{k+1} = f(x_k, u_k, w_k)$$
$$y_k = h(x_k, v_k) \tag{70}$$

where w_k, v_k are the state and measurement noise vectors respectively. The EKF is a recursive algorithm operates in two steps: prediction step and update step.
Prediction step:

$$\bar{x}_{k+1} = f(\hat{x}_k, u_k, 0)$$
$$\bar{P}_k + 1 = A_k P_k A_k^T + Q_k \tag{71}$$

where P_k is the state error covariance, Q_k is the covariance of state noise, A_k is the Jacobian of $f(x_k, u_k, w_k)$.
Update step:

$$x_{k+1} = \bar{x}_{k+1} + K_{k+1}\left(Z_{k+1} - h(\bar{x}_{k+1})\right)$$
$$P_{k+1} = (I - K_{k+1}H_k)\bar{P}_{k+1} \tag{72}$$

where K_k is the Kalman gain that minimizes the estimation error.
Hence, the estimated vertical forces are given by

$$\hat{F}_{zf(k+1)} = \hat{F}_{zf(k)} + \Delta T/(m_s + m_u)\Big((m_s + m_u)g - $$
$$(m_s + m_u)(\hat{v}_{(k)} + g\hat{\theta}_{s(k)})\hat{h}_{f(k)}/2(L_f + L_r) + m_s\hat{z}_{s(k)} + $$
$$m_u\hat{z}_{u(k)}\Big) \tag{73}$$

$$\hat{F}_{zr(k+1)} = \hat{F}_{zr(k)} + \Delta T/(m_s + m_u)\Big((m_s + m_u)g - $$
$$(m_s + m_u)(\hat{v}_{(k)} + g\hat{\theta}_{s(k)})\hat{h}_{r(k)}/2(L_f + L_r) + m_s\hat{z}_{s(k)} + $$
$$m_u\hat{z}_{u(k)}\Big)$$

where ΔT is the sampling time.

Remark 7: *$\ddot{z}_u$ in the suspension system is measured by the suspension deflection sensors and$\ddot{z}_s$ is calculated by (50). $\dot{v}$ and θ_s are provided by the AHSMO. The 6D-IMU unit produces the pitch and roll rate $\dot{\theta}, \dot{\phi}$ respectively. The heights of the CoG from the front and rear wheel are updated as $\hat{h}_f \approx h_f + \partial R_{ef}$ and $\hat{h}_r \approx h_r + \partial R_{er}$, where ∂R_e is the change in the effective tyre radius.*

Magic Formula parameter estimation

The Magic Formula parameters defined by equation (63) are updated using an EKF and tuned based on experimental tyre data to obtain the μ-λ curve beyond the maximum point to describe high-slip conditions.

The tyre force model (63) is now defined as

$$x_{k+1} = f(a_k, u_k) + \omega_k$$

$$a_{k+1} = f(a_k, u_k) + \omega_k \tag{74}$$

$$z_k = h(a_k) + v_k$$

For this system, the parameters a_k can be estimated by means of the following equations
Time update:

$$a_{k+1} = a_k$$

$$P_{k+1}^- = S_k \tag{75}$$

Measurement update

$$K_k = P_k^- H_k^T \left(H_k P_k^- H_k^T + R_k \right)^{-1}$$

$$\hat{a}_k = \hat{a}_k^- + K_k \left(z_k - h(\hat{a}_k^-) \right) \tag{76}$$

$$P_k = (I - K_k H_k) P_k^-$$

where

$$H_k = \frac{\delta h(\hat{a}_k)}{\delta a}$$

Remark 8: *$\widehat{\lambda}$ data obtained from the HSMO, experimental tyre data and the estimated F_z are used to update the MF parameters.*

Hence, improved estimation of frictional force (63) is achieved even during high-slip conditions and the estimated frictional force is given by

$$\hat{F}_x = \hat{D}_p \sin\left(\hat{C} \tan^{-1}\left(\hat{B}\left((1 - \hat{E})\hat{\lambda} + \left(\frac{\hat{E}}{\hat{B}}\right) \tan^{-1}(\hat{B}\hat{\lambda}) \right) \right) \right) \tag{77}$$

Optimal slip generation

Finally, for effective ABS control, the optimal slip λ^d must be generated. The maximum

braking force will be generated at the optimal slip. Therefore, one can determine

$$\frac{dy}{dx}\Big|_{(x=\lambda^d, y=F_x)} = 0 \tag{78}$$

From equation (63)

$$\frac{dy}{dx} = \frac{BCD_p}{(1 + [Bx(1-E) + E\ arctan(Bx)]^2)} \tag{79}$$

Equations (78) and (79) yield

$$Cos(C\ arctan[B\lambda^d(1-E) + E\ arctan(B\lambda)]) = 0 \tag{80}$$

Therefore, the optimized slip can be expressed as

$$\lambda^d = \frac{\tan(0.5)\,\pi/C - E\ arctan(B\lambda)}{B(1-E)} \tag{81}$$

Summary of the two schemes

The proposed schemes not only explore the influences of wheel, suspension and vehicle dynamics in accurate estimation of slip and tyre forces but also present insight into the relative merits of using either an HSMO or a SMO in the proposed cascaded structure. The HSMO scheme estimates vehicle velocity and road slope together eliminating any uncertainty or disturbances caused by any coupling between dynamics. Conversely, the SMO scheme calculates the road slope first using available measurements then uses it to estimate vehicle velocity. Furthermore, the SMO only considers a linear $\mu - \lambda$ relationship and has increased dependency on available sensors. It is demonstrated that the dynamic coupling between the sub-systems, together with model and sensor requirements, impact on the paradigm for efficient slip and friction estimation.

5. SIMULATION TESTS

Two braking scenarios are simulated using the full car nonlinear model presented in section 4.1 to validate the presented estimation schemes. Both schemes are compared and the HSMO is also benchmarked against an adaptive Kalman Filter (KF) scheme [57] which is designed to estimate vehicle velocity and road slope within the framework of Figure 19. The side slip and lateral forces are estimated using an EKF for yaw control during braking and cornering. The yaw control system used in the simulation testing is presented in the Appendix. The sliding Mode Control (SMC) based ABS controller from [58] has been used in the simulations. The controller tracks the desired slip λ_d generated by the optimal slip generator

Two braking cases have been considered: braking on a surface where μ changes from a low value to a high value as well as a critical braking and cornering scenario. Each case is described in detail below with full simulation results presented. Except for the response of the front and rear vertical forces, only left rear wheel responses are given. This is because the Root Mean Square (RMS) error corresponding to estimation of the front and rear longitudinal force, effective tyre radius and slip are in the same range. A summary of the Root Mean Square (RMS) error will instead be provided.

Case 1

Braking is performed from 30 m/s on a surface where μ changes from 0.2 to 0.9 after 5 seconds. Road slope is increased from 18 to 20 % at the 5th second. No steering input is given

so that $\delta = 0$; effectively the yaw control system is disabled. The results are shown in Figure 21 where the figures compare the actual signal with the estimates obtained using the SMO, the HSMO and the KF approaches. The vehicle velocity estimated by the SMO exhibits a large deviation on the low μ surface with the error reducing on the high μ surface (Figure 21a). Furthermore, oscillations are induced in the vehicle velocity estimated by the KF. The HSMO produced accurate estimation of vehicle velocity before and after the split. Indeed, the HSMO produced better estimation of vehicle velocity (Figure 21a), slip (Figure 21b) and longitudinal force (Figure 21c) demonstrating a clear ability to adapt to varying road conditions. The calculated road slope is shown in Figure 21f. The SMO exhibits oscillatory behaviour and considerable deviation throughout the manoeuvre. Accuracy of estimated effective tyre radius (Figure 21g) and vertical force estimates (Figures 21d and 21e) by the SMO and KF schemes is less accurate when compared to the HSMO case and increased deviation appears after the split.
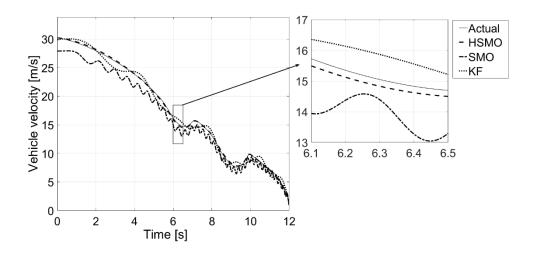
Figure 21a. Longitudinal velocity case 1
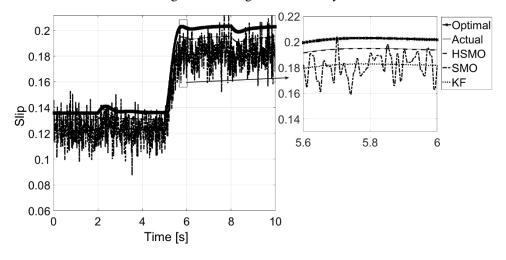
Figure 21b. Slip case 1
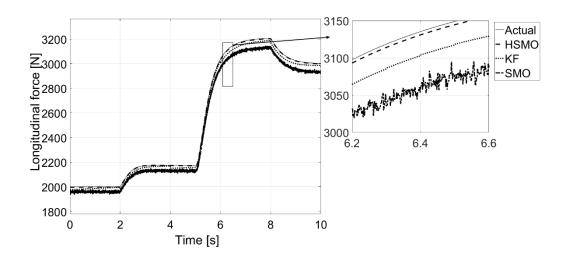
Figure 21c. Longitudinal force case 1
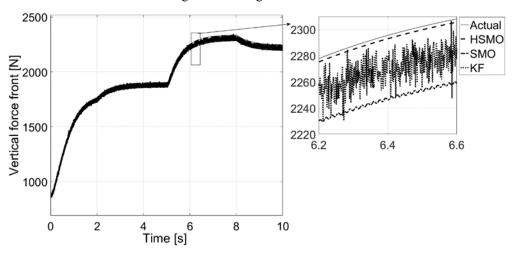
Figure 21d. Vertical force front case 1
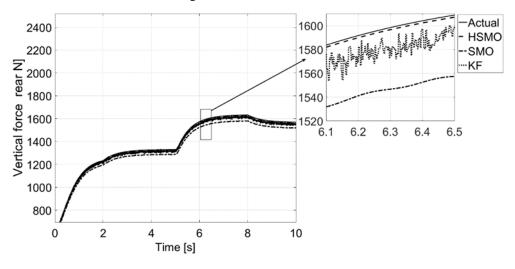
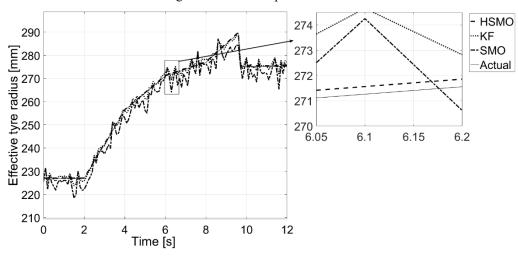Figure 21e. Vertical force rear case 1
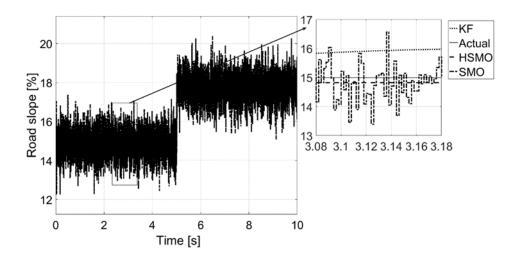
Figure 21f. Road slope case 1

Figure 21g. Effective tyre radius case 1

Case 2

A combined braking and cornering manoeuvre is performed from 40 m/s on a surface where $\mu = 0.2$ changes to $\mu = 0.8$ after 2 seconds and the road slope is varied from 20 to 15%. The results are shown in Figure 22. Figure 22a shows the braking path. The vehicle velocity is shown in Figure 22b where it is seen that the estimates from the SMO and KF exhibit large deviations when compared to the HSMO. Furthermore, the velocity responses of both the SMO and KF are oscillatory with the oscillations exhibited by the SMO being the most intense. Estimation of the longitudinal force (Figure 22d) by both the SMO and KF shows high inaccuracy. The SMO performance decreases substantially from Case 1 to Case 2. Calculation of road slope (Figure 22g) and estimation of effective tyre radius (Figure 22h) by both the SMO and KF are highly oscillatory and the error in the vertical force estimation (Figure 22e and 22f) increases compared to case 1. In comparison the HSMO produced very good results overall in what is a challenging braking scenario.
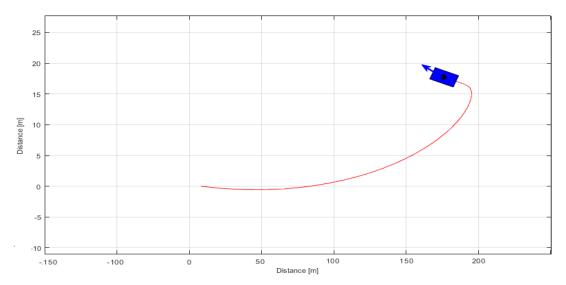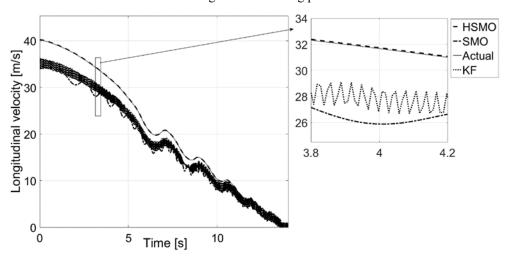
Figure 22a. Braking path

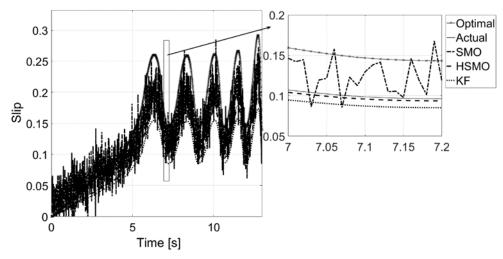
Figure 22b. Longitudinal velocity case 2
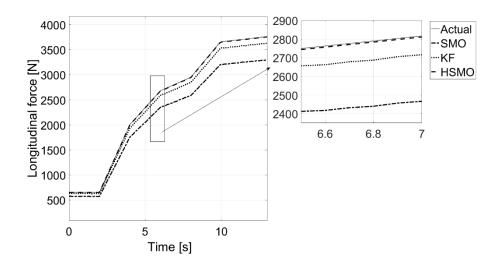

Figure 22c. Slip case 2
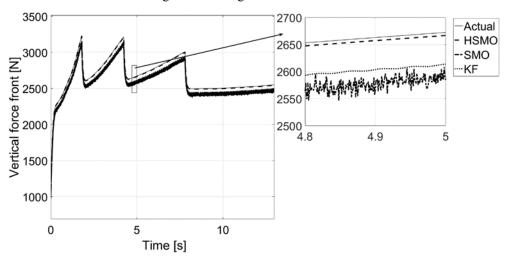
Figure 22d. Longitudinal force case 2

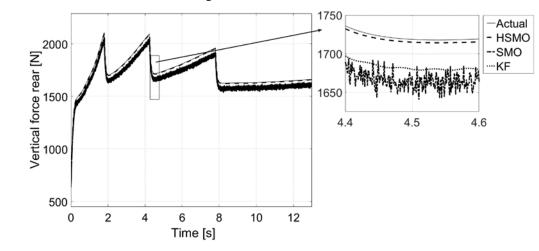Figure 22e. Vertical force front case 2
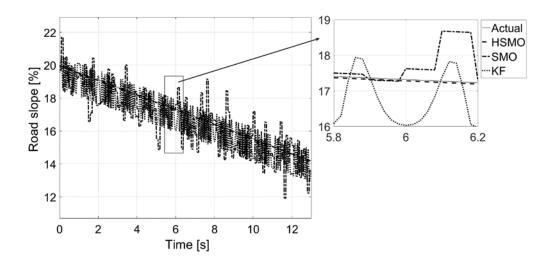

Figure 22f. Vertical force rear case 2
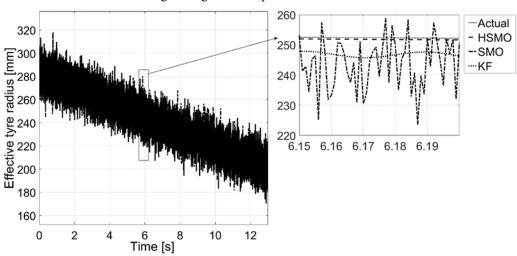
Figure 22g. Road slope case 2

Figure 22h. Effective tyre radius case 2

The results of the simulation tests are summarised in Figure 23 below where the Root Mean Square (RMS) error between the estimated and actual states and parameters are presented for the HSMO, SMO and KF. The HSMO is seen to exhibit high adaptability and robustness to variations in road conditions and uncertainties in the vehicle dynamics.
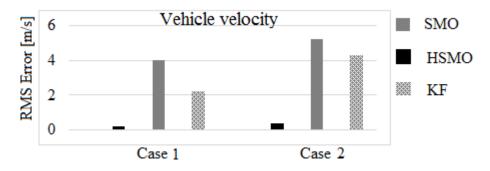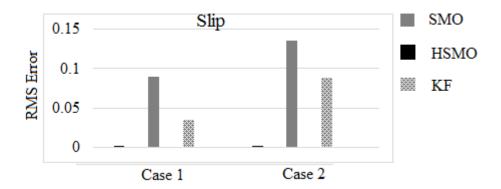

Figure 23a. RMSE vehicle velocity
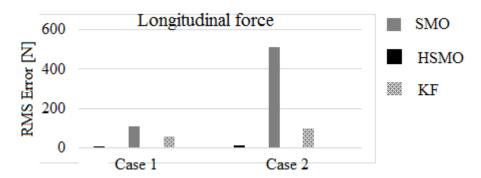
Figure 23b. RMSE Slip
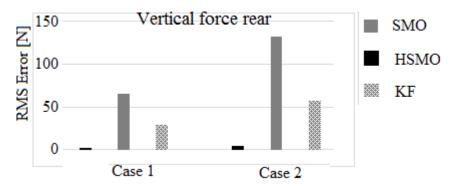

Figure 23c. RMSE Longitudinal force
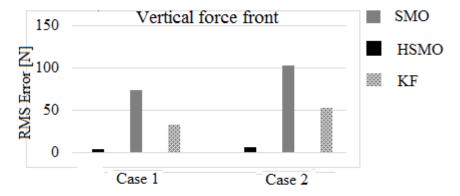

Figure 23d. RMSE Vertical force rear
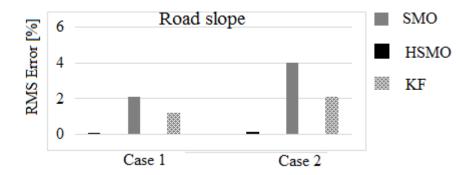

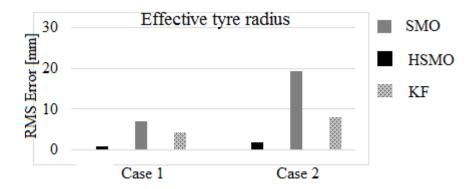Figure 23e. RMSE Vertical force front

Figure 23f. RMSE road slope

Figure 23g. RMSE Effective tyre radius

6. CONCLUSIONS

Although both the HSMO and SMO schemes capture the influences of the vehicle dynamics, wheel dynamics and suspension dynamics in the proposed cascaded structure, the HSMO demonstrated better robustness overall to any disturbances and uncertainties. This is because the SMO has been developed based on a linear $\mu - \lambda$ relationship and it is assumed it is valid over a small slip range. Furthermore, the SMO scheme depends on accurate measurements. The HSMO also exhibited very good performance when compared to the KF where the KF was used in the same cascaded scheme. Even though the scheme produced very good performance with a full car model in the Matlab/Simulink environment for critical braking cases, experimental validation is required. Furthermore, suspension dynamic influences have not been fully analysed since no road profile changes (bumps, potholes) are considered. Such road profile changes and associated influences and variation in CoG position will be explored in detail in future work. Furthermore, although the impact of the yaw dynamics has been considered extensively in testing, the impact of the complete lateral dynamics including rolling effects has not been explored. Hence, in future work the impact of road bank angle will also be considered.

REFERENCES

1. Robert Bosch GmbH., Konrad Reif, and Karl-Heinz Dietsche. Automotive handbook. Robert Bosch GmbH, 2014.
2. Y. Gao and M. Ehsani, "Electronic Braking System of EV and HEV – Integration of Regenerative Braking, Automatic Braking Force Control and ABS", SAE International, DOI 10.4271/2001-01-2478, 2006.

3. S. Hano and M. Hakiai, "New Challenges of Brake and Modulation Systems in Hybrid Electric Vehicles (HEVs) and Electric Vehicles (EVs)", *SAE International*, DOI:10.4271/2011-39-7210, May 2011.

4. Bo-Rong Liang; Wei-Song Lin, "A new slip ratio observer and its application in electric vehicle wheel slip control", *IEEE International Conference on Systems, Man, and Cybernetics (SMC)*, pp.41,46, Oct 2012.

5. I. Petersen, T. A. Johansen, J. Kalkkuhl, and J. Lüdemann, "Wheel slip control in ABS brakes using gain scheduled constrained LQR", in *European Control Conference*, Porto, 2001.

6. M. Amiri, B. Moaveni, "Vehicle Velocity Estimation based on Data fusion by Kalman Filtering for ABS", *20th Iranian Conference on Electrical Engineering*, 15-17 May 2012.

7. D. M. Bevly, J. C. Gerdes, and C. Wilson, "The use of GPS based velocity measurements for measurement of sideslip and wheel slip", *Vehicle Systems and Dynamics*, vol. 38, no. 2, pp. 127–147, Aug. 2002.

8. Cornelia Lex. "*Estimation of the Maximum Coefficient of Friction between Tire and Road Based on Vehicle State Measurements*", PhD Thesis, Graz University, 2015.

9. A.A.A. Salih, N.L.A.C.A. Zaini, and A. Zhahir. "The Suitability of GPS Receivers Update Rates for Navigation Applications", *World Academy of Science, Engineering and Technology*, 7(6):214–221, 2013.

10. G. Genta, "Motor vehicle dynamics: modeling and simulation", Vol. 43. World Scientific, 1997.

11. F. Jiang, "A novel control approach to a class of antilock brake problems", PhD thesis, Cleveland State University, 2000.

12. S. M. Savaresi and M. Tanelli, "Active braking control systems design for vehicles". Springer Science & Business Media, 2010.

13. J.Y. Wong, "Theory of ground vehicles", 4th Ed, *John Wiley & Sons Inc.,* ISBN: 13:978-0470170380, 2008.

14. G. Mastinu, M. Ploechl, "Road and offroad vehicle system Dynamics handbook", *CRC Press*, ISBN: 13:978-0-8493-3322-4, 2014.

15. C. Liang, R. W. Allen, T. Rosenthal, J. Chrstos , "Tire Modeling for Off-Road Vehicle Simulation," *SAE Technical Paper 2004-01-2058*, DOI: 10.4271/2004- 012058, 2004.

16. L. Bin, X. Yang, and J. Yang. "Tire model application and parameter identification-A literature review." *SAE International Journal of Passenger Cars-Mechanical Systems*,7.2014-01-0872: 231-243, 2014.

17. H. Pacejka, "Tyre and vehicle dynamics", *Book, 2nd Edition. SAE International*, 2005.

18. W. Milliken, D. Milliken, and L. Metz, "Race car vehicle dynamics", *SAE International* 1995.

19. T. Gillespie, "Fundamentals of Vehicle Dynamics," *SAE International*, 1992.

20. V. Ivanov, B. Shyrokau, K. Augsburg, and V. Algin, "Fuzzy evaluation of tyre-surface interaction parameters", *Journal of Terramechanics*, 47(2):113–130, 2010.

21. B. Breuer, M. Barz, K. Bill, S. Gruber, M. Semsch, T. Strothjohann, and C. Xie, "The Mechatronic, Vehicle Corner of Darmstadt University of Technology - Interaction and Cooperation of a Sensor Tire, Low-Energy Disc Brake and Smart Wheel Suspension" *International Journal of Automotive Technology* 3(2):63–70, 2002.

22. B. Breuer, T. Bachmann, S. Ernesti, and J. Stocker, "Methods and Instruments for On-Board Measurement of Tyre/Road Friction". *SAE technical paper,* 942470, 1994.

23. M. R. Uchanski. "Road friction estimation for automobiles using digital signal processing methods" Dissertation thesis, University of California, Berkeley. 2001.

24. C. Lex, H. Kobialka, and A. Eichberger, "Identification of the friction potential for the application in an automated emergency braking system. In *Proceedings of 13th Stuttgart International Symposium*, volume 2, pages 55–69. Springer Vieweg, 26-27. Stuttgart, Germany, 2013.

25. S.A. Chang ."Robust estimation of road friction coefficient for vehicle active safety systems", PhD Thesis, University of Michigan. 2001.

26. J.E. Bowman, E.H. Law, "A Feasibility Study of an Automotive Slip Control Braking System", *SAE technical paper* 930762, 1995.

27. B. Ma, H. Guo, H. Zhang, H. Chen and Z. Sun, "Estimation of road grade and vehicle velocity for autonomous driving vehicle", *Industrial Electronics Society IECON 2017 - 43rd Annual Conference of the IEEE*, pp.4621 4626, 2017.

28. K. Kobayashi, K. C. Cheok and K. Watanabe, "Estimation of Absolute Vehicle Speed using Fuzzy Logic Rule-Based Kalman Filter*", Proceedings of the American Control Conference*, Seattle, Washington, p 3086-3090, 1995.

29. L. R. Ray. 1992. "Nonlinear Estimation of Vehicle State and Tire Forces", *Proceedings of the American Control Conference*, Chicago, Illinois, p 526-530.

30. F. Jiang and Z. Gao, "An Adaptive Nonlinear Filter Approach to the Vehicle velocity Estimation for ABS" *IEEE Transaction on Automtic control*, pp.490-49, 2000.

31. D. Kun, L. Kaijun, and X. Qunsheng, "Application of Unscented Kalman Filter for the State Estimation of Anti-lock Braking System" *IEEE*, Tshinghua University, 2006.

32. A. Melika, "designing of optimum filtering structure in order to linear speed estimation of vehicle for ABS" thesis of MA, Islamic azad university science and research, p 22-35, 2006.

33. A. Daiss and U. Kiencke, "Estimation of Vehicle Speed Fuzzy-Estimation in Comparison with Kalmn Filtering", *Proceedings of the 4th IEEE Conference on Control Applications*, Albany, New York, p 281-284,1995.

34. T. Dieckmann "The tire slip as an indicator for the adhesion potential", Dissertation PhD. Hannover

University. 1992.

35. F. Gustafsson, "Monitoring tire-road friction using the wheel slip," *IEEE Control Systems Magazine,* vol. 18, pp. 42-49, 1997.

36. L. R. Ray, "Nonlinear Tire Force Estimation and Road Friction Identification: Simulation Experiments". *Automatica*, 33:1819–1833, 1997.

37. B. Boßdorf-Zimmer, L. Frömmig, R. Henze, and F. Küçükay, "Real Time-Processing Vehicle State Estimation". In *Proceedings of chassis. tech*. Springer Vieweg, 1-2. Munich, Germany, 2007.

38. C. Lee, K. Hedrick, and J. Yi, "Real-time slip-based estimation of maximum tire-road friction coefficient". *IEEE/ASME Transactions on Mechatronics*, 9(2):454–458, 2004.

39. J. Yi, L. Alvarez, X. Claeys and R. Horowitz." Emergency braking control with an observer-based dynamic tyre/road friction model and wheel angular velocity measurement. *Vehicle System Dynamics*, 39:81–97, 2003.

40. N. Patel, C. Edwards and S.K. Spurgeon, 'A Sliding Mode Observer for Tyre Friction Estimation During Braking', Proceeding of the American Control Conference, Minneapolis, pages 5867-5872, 2007.

41. N. Patel, C. Edwards and S.K. Spurgeon, 'Tyre/road Friction Estimation using a Sliding Mode Based Observer', Volume 7, Part 1, 7th IFAC Symposium on Nonlinear Control Systems, Pretoria, South Africa August 2007.

42. N. Patel, C. Edwards and S.K. Spurgeon, 'Optimal Braking and Estimation of Tyre Friction of Automotive Vehicles Using Sliding Modes', International Journal of Systems Science special issue on Advances on Sliding Mode Observation and Estimation' Volume 38, Issue 11, Pages 901-912, 2007.

43. M. Tanelli, L. Piroddi, and S.M. Savaresi, "Real-time identification of tyre-road friction conditions," *IET Control Theory & Applications*, vol. 3, no. 7, pp. 891–906, 2009.

44. M. Tanelli, S.M. Savaresi, and C. Cantoni, "Longitudinal Vehicle Speed Estimation for Traction and Braking Control Systems," in *Proceedings of the Conference on Control and Applications – CCA*, Munich Germany, 2006.

45. S. Koskinen and P. Peussa, FRICTION, Final Report - Public. Deliverable 13 for the *European commission*, *Technical Research Centre* (VTT), Tampere, Finland, 2009.

47. N.K. M'sirdi, A. Rabhi, L. Fridman, J. Davila, and Y. Delanne, "Second order sliding mode observer for estimation of velocities, wheel slip, radius and stiffness," American Control Conference Minneapolis, USA, June 14-16, pp.3316–3321, 2006.

48. J. Davila, L. Fridman, and A. Levant, "Second-order sliding-mode observer for mechanical systems," *IEEE Transactions on Automatic Control*, vol. 50, no. 11, pp. 1785–1789, 2005.

49. R. Rajamani, G. Phanomchoeng, D. Piyabongkarn and J. Y. Lew, "Algorithms for Real-time Estimation of Wheel Tire-Road Friction Coefficient". *IEEE/ASME Transactions on Mechatronics*, 17(6):1183–1195, 2012.

50. R. Rajamani, D. Piyabongkarn, J. Y. Lew, and J. A. Grogg, "Algorithms for real-time estimation of individual wheel tire-road friction coefficients", in *Proceedings of American Control Conference (ACC)*, pages 4682–4687. *IEEE* Computer Society, 14-16. Minneapolis, Minnesota, USA, 2009.

51. L. Imsland, T.A. Johansen, T.I. Fossen, J.C. Kalkkuhl, and A. Suissa, "Vehicle Velocity Estimation using Modular Nonlinear Observers", in *Proceedings of 44th Conference on Decision and control and the European Control Conference*, pages 6728–6733, *IEEE Computer Society*, 12-15 December 2005.

52. C.E. Tannoury, F. Plestan, S. Moussaoui and N. Romani, "Tyre effective radius and vehicle velocity estimation: a variable structure observer solution", *8th International Multi-Conference on Systems, Signals and Devices (SSD)*, Sousse, Tunisia, DOI:10.1109/SSD.2011.5767491, 22-25 March 2011.

53. M. Tanelli, A. Ferrara, and P. Giani, ''Combined vehicle velocity and tire-road friction estimation via sliding mode observers,'' in *Proc. IEEE Int. Conf. Control Appl. (CCA)*, pp. 130–135, October 2012.

54. R. Tafner, M. Reichhartinger and M. Horn, ''Estimation of tire parameters via second-order sliding mode observers with unknown inputs,'' in *Proc.13th Int. Workshop Variable Struct. Syst. (VSS)*, pp. 1–6, 2014.

55. E. Regolin, M. Zambelli and A. Ferrara, "Wheel Forces Estimation via Adaptive Sub-Optimal Second Order Sliding Mode Observers,". *International Conference on Information, Communication and Automation Technologies (ICAT),* 2017.

56. A. Levant, "Sliding order and sliding accuracy in sliding mode control", *International Journal of Control,* 58 (6) 1247–1263, 1993.

57. M. Klomp, Y. Gao and F. Bruzelius, "Longitudinal velocity and road slope estimation in hybrid electric vehicles employing early detection of excessive wheel slip". *Vehicle System Dynamics*; 52(Suppl): 172–188, 2014.

58. S. Rajendran, S. Spurgeon, G. Tsampardoukas and R. Hampson, "Time-varying sliding mode control for Electric Car (EC)" *20th IFAC World Congress,* Toulouse, France, Vol. 50, issue 1, Pages 8490-8495, 2017.

59. H. Pacejka and R. Sharp, "Shear Force Development by Pneumatic Tyres in Steady State Conditions: A Review of Modelling Aspects," *Vehicle System Dynamics*, vol. 20, no. 3-4, pp. 121–175, Jan 1991.

60. H. Imine and L. Fridman, "Estimation of the Unknown Inputs and Vertical Forces of the Heavy Vehicle Via Higher Order Sliding Mode Observer", *IEEE Intelligent Vehicles Symposium, IEEE,* pp.949 – 954, Istanbul, Turkey, June 2007.

61. H. Imine and V. Dolcemascolo, "Vertical tyre forces estimation to calculate the Rollover risk of heavy

Vehicles", *FISITA'06, World Automotive Congress*, Yokohama, Japan, 22 - 27 October 2006.

62. H. Imine, V. Dolcemascolo and B. Jacob, "Influence of the road profile on wheel and vehicle loads estimation", *9th International Symposium on Heavy Vehicle Weights and Dimensions, ISHVWD'09*, Pennsylvania, USA June 2006.

63. H. Imine, A. Benallegue, T. Madani, and S. Srairi, "Rollover risk prediction of an instrumented heavy vehicle using high order sliding mode observer", in *Proceedings of International Conference of Robotics and Automation, ICRA*, Kobe, Japan, May 12 – 17, 2009.

64. H. Imine, S. Srairi and T. Madani, "Experimental validation of rollover risk prediction of heavy vehicles", TRA'08, Transport Research Arena, Ljubljana, Slovenia, 21-25 April 2008.

65. H. Imine, O. Khemoudj, M. Djemai and K. Busawon, "Robust observer design of tire forces in heavy-duty vehicles", *IEEE transactions on intelligent transportation systems,* vol. 16, no. 6, pp. 3304 – 3312, 2015.

66. H. Imine, L Fridman, H. Shraim and M. Djemai. "Sliding Mode Based Analysis and Identification of Vehicle Dynamics", *Springer Verlag, Lecture Notes in Control and Information Sciences*, v. 414, ISBN 978-3-642-22224-5, 2011.

67. A. Ferrara, "Sliding Mode Control of Vehicle Dynamics", *IET*, ISBN: 978-1-78561-209-7, 2017.

68. A. Chalanga, S. Kamal. L. Fridman, J. Moreno and B. Bandyopadhyay, "Implementation of Super-Twisting Control: Super-Twisting and Higher Order Sliding Mode Observer Based Approaches", *IEEE Transactions on Industrial Electronics*, Vol. 63, No. 6, pp. 3677 - 3685, DOI: 10.1109/TIE.2016.2523913, 2016.

69. J. A. Moreno and M. Osorio, "Strict Lyapunov functions for the super-twisting algorithm", *IEEE Transactions on Automatic Control*, vol.57, no.4, pp.1035-1040, 2012.

70. N. K. M'sirdi, A. Rabhi, M. Ouladsin and L. Fridman, "First and high-order sliding mode observers to estimate the contact forces", in *Variable Structure Systems, VSS'06, International Workshop on, IEEE*: 274–279, 2006.

71. W. Hirschberg, G. Rill, and H. Weinfurter. "Tire model TMeasy", *Vehicle System Dynamics*, 45(Suppl. 1):101–119, 2007.

APPENDIX

Integrated yaw control for manoeuvres in curve

To perform braking in a curve, both yaw rate and side slip play an important role. A typical integrated yaw control system is given in Figure 24. For an effective lateral control system, the side slip angle β should be maintained at a desired value β_d to achieve lateral stability and it is not measurable directly in reality. Hence, estimation of β is required. The lateral velocity v_y is needed to estimate β and accurate estimation of β in braking or acceleration depends on the longitudinal forces. Therefore, an EKF is designed based on the full car model described in section 4.1 to estimate lateral velocity and side slip.
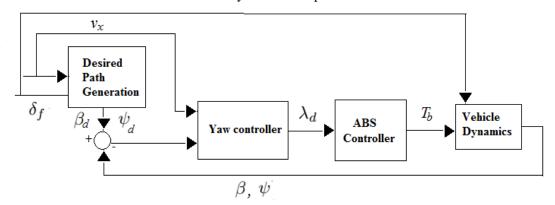

Figure 24. Integrated control system

The state vectors x_k, u_k and y_k of the EKF are given as

$$x_k = \begin{bmatrix} v_{x,k} & v_{y,k} & \dot{\psi} & F_{y,k}^{ij} & C_s^{ij} \end{bmatrix}^T$$

$$u_k = \begin{bmatrix} \delta_k^{ij} & F_{x,k}^{ij} \end{bmatrix}^T$$

$$y_k = \begin{bmatrix} v_{x,k} & a_{y,k} & \dot{\psi}_k \end{bmatrix}^T$$

where $ij = fR, fL, rR, rL$

Remark 9: *The longitudinal vehicle velocity v_x, and the longitudinal force F_x are provided by the designed observer schemes and the lateral acceleration a_y and yaw rate $\dot{\psi}$ are measured by the IMU, respectively. Furthermore, it is assumed that the road bank angle is zero.*

A PID based yaw controller is designed based on the following linear system.

$$\dot{x} = Ax + Bu$$

where

$$x = \begin{bmatrix} \beta & \dot{\psi} \end{bmatrix}^T$$

$$u = \delta$$

$$A = \begin{bmatrix} -\dfrac{2C_s^f + 2C_s^r}{mv_x} & -\dfrac{2C_s^f l_f - 2C_s^r l_r}{mv_x^2} - 1 \\ -\dfrac{2C_s^f l_f - 2C_s^r l_r}{I} & -\dfrac{2C_s^f l_f^2 + 2C_s^r l_r^2}{Iv_x} \end{bmatrix} \text{ and } B = \begin{bmatrix} \dfrac{2C_s^f}{mv_x} \\ \dfrac{2C_s^f l_f}{I} \end{bmatrix}.$$